

Research paper

A novel strategy for multitype fault diagnosis in photovoltaic systems using multiple regression analysis and support vector machines

Shiue-Der Lu^a, Hwa-Dong Liu^{b,*}, Meng-Hui Wang^a, Chia-Chun Wu^a^a Department of Electrical Engineering, National Chin-Yi University of Technology, Taichung 411, Taiwan^b Undergraduate Program of Vehicle and Energy Engineering, National Taiwan Normal University, Taipei 106, Taiwan

ARTICLE INFO

Keywords:

Solar power system
Fault diagnosis
Multiple regression analysis
Support vector machines

ABSTRACT

This study focuses on analyzing common fault types in photovoltaic (PV) modules, employing fault diagnosis methods based on machine learning technology to enhance the accuracy and efficiency of diagnosing faults in solar power systems. Initially, we collected relevant data from the solar power system and used data analysis techniques to identify system faults, designing a human-machine monitoring interface for practical application. Furthermore, the experimental results proved that the system could accurately identify eight major types of faults, including solar panel output circuits, energy storage batteries, maximum power point tracking (MPPT) controllers, inverters, dust accumulation, loosening of mounting rack screws, damage to the mounting rack foundation, and deformation of the mounting rack structure. Particularly in the detection of dust accumulation, we developed a new method of estimating power generation from multiple regression analysis (MRA), which closely aligns the estimated power output with the actual power output, highlighting the significant impact of dust accumulation on the efficiency of solar power systems. Next, by integrating voltmeters and support vector machines (SVM) into the solar PV array modules, we are able to quickly and accurately measure and locate short-circuit and open-circuit faults in bypass diodes. Ultimately, the proposed PV fault diagnosis strategy includes diagnostics for dust accumulation and mounting frame faults, making it particularly suitable for areas with severe air pollution and frequent earthquakes, providing a comprehensive fault diagnosis solution.

1. Introduction

In light of the significant global energy crisis, the 27th (COP27 in 2022) (Khalil and Zeid, 2023; Salam et al., 2023) and 28th (COP28 in 2023) United Nations Climate Change Conferences were convened. Governments globally are actively devising and promoting strategies for carbon reduction, including: (i) Employing low-carbon emission techniques for oil extraction, while gradually reducing reliance on petrochemical fuels. (ii) Vigorously advocating for an energy transition towards clean energy, with the goal of significantly reducing greenhouse gas emissions before 2030. (iii) Implementing schemes to compensate for climate-related losses and damages. These annual United Nations Climate Change Conferences serve as platforms to review and evaluate these strategies, fostering advancements in greenhouse gas mitigation and the enactment of carbon reduction policies to address extreme weather events and global warming. Thus, the development of renewable energy is imperative. The spectrum of renewable energy encompasses a variety of sources, including solar (Oni et al., 2024; Cabral et al.,

2024), wind, hydro, biomass, and geothermal energy. This research specifically concentrates on solar power systems due to their benefits, such as absence of noise pollution, longevity, and low maintenance requirements (Amer et al., 2023; Zaidi, 2024).

The development of solar energy systems has witnessed remarkable progress and expansion, reflecting a global shift towards renewable energy sources. This transition is driven by the need to meet increasing energy demands sustainably, reduce dependency on fossil fuels, and mitigate environmental impacts. Below is a selection of international journal papers that illustrate various facets of solar energy system development: (i) Solar energy technology and its roles in sustainable development: This paper highlights the job creation potential of solar photovoltaic (PV) applications across various countries, emphasizing the significant role of solar energy in sustainable development by reducing carbon emissions without hindering national development. It underscores the abundant solar energy potential in "Sunbelt" countries, which can significantly contribute to solar energy technology development due to their high solar irradiation levels (Maka and Alabid, 2022).

* Corresponding author.

E-mail addresses: SDL@ncut.edu.tw (S.-D. Lu), hdliu@ntnu.edu.tw (H.-D. Liu), wangmh@ncut.edu.tw (M.-H. Wang), wu1998117@gmail.com (C.-C. Wu).

Table 1

Comparison of detection items for four PV fault diagnosis strategies.

Detection items	(Alwar et al., 2022)	(Selvaraj et al., 2022)	(Liu et al., 2023)	Proposed
Dust accumulation levels on the surface of PV panels	Not diagnosable	Not diagnosable	Not diagnosable	Diagnosable
Faults in PV panel mounting brackets	Not diagnosable	Not diagnosable	Not diagnosable	Diagnosable
Faults in PV electrical devices	Diagnosable	Diagnosable	Diagnosable	Diagnosable

(ii) Advancements in solar panel technology in civil engineering: Focused on the last 15 years of research, this review explores the integration of solar panels into building designs and their role in innovative infrastructure applications like photovoltaic parking lot canopies and noise barriers. It discusses solar panels' contributions to energy efficiency, water management systems, urban planning, and building materials, underscoring solar energy's versatility in construction (Vijayan et al., 2023). (iii) Solar energy: Applications, trends analysis, bibliometric analysis and research contribution to sustainable development goals (SDGs): Analyzing 126,513 papers from 2011 to 2021, this paper discusses the utilization of solar PV systems in various applications, including large-scale and residential solar PV, green hydrogen production, water desalination, and transportation. It notes a research gap in solar energy related to several SDGs, indicating areas for further exploration (Obaideen et al., 2023). (iv) Recent advances in solar PV materials and systems for energy storage applications: This review delves into solar PV systems' applications and categorizations, highlighting their role in grid-connected and stand-alone systems. It examines the advantages of grid-tied solar PV systems, their cost-effectiveness, simple design, and low maintenance requirements, and the potential of off-grid PV systems with battery storage for daytime electricity generation (Dada and Popoola, 2023). (v) A review of solar energy - the world bank: This comprehensive review addresses solar energy technologies, markets, and policy approaches to enhance solar energy development. It discusses the impacts of greenhouse gas mitigation policies on solar energy deployment, providing a global perspective on solar energy's current status and future potential (Govinda et al., 2011). These papers represent a fraction of the extensive research being conducted in the field of solar energy, highlighting advancements in technology, applications, and the significant role of solar power in achieving sustainable development goals. The ongoing research and development in solar energy technology hold promise for a cleaner, greener future, showcasing the critical role of solar power in the global energy transition.

The research field of solar energy systems is extensive, especially after the completion of system installations that are intended to supply power over long periods to users with demand. At this stage, the stability of the solar energy system becomes particularly critical. Therefore, this study primarily focuses on the fault diagnosis mechanisms of solar energy systems. Furthermore, the fault diagnosis mechanisms currently explored by researchers encompass the following aspects: Fault detection in solar energy systems through a deep learning approach - This research investigates the application of deep learning for identifying defects in photovoltaic panels via infrared images of solar modules. Utilizing a dataset comprising 20,000 images that encapsulate a variety of defect types, the study leverages the EfficientNetB0 model and an support vector machine (SVM) classifier, attaining remarkable accuracy, F1-score, precision, and sensitivity metrics in the classification of photovoltaic panel defects (Duray, 2023). Artificial neural network for fault diagnosis of solar PV systems: A survey - This paper provides a comprehensive review of the application of artificial neural networks

(ANN) in diagnosing faults in PV systems. Covering a variety of ANN models and examining their input attributes, fault types, and diagnostic performance, the survey highlights the challenges and development trends in applying ANN for PV system fault diagnosis (Yuan et al., 2022). Development of a machine-learning-based method for early fault detection in PV systems - Focusing on early fault detection, this paper discusses a machine-learning-based method that can identify a wide range of faults using the kernel-based extreme learning machine (KELM) and data from current-voltage (I-V) curves to identify a wide range of faults. The approach emphasizes the importance of early and accurate fault detection to prevent energy loss and ensure the safety of PV system installations (Voutsinas et al., 2023). Additionally, research on solar power systems has developed a fault classifier and reconfiguration algorithm based on thermal imaging analysis, effectively enhancing the power output of partially shaded solar systems due to hotspots, partial shading, and other minor faults (Alwar et al., 2022). Aging of PV panels, primarily caused by environmental and electrical faults, is addressed by finely tuning a pre-trained convolutional neural network (CNN) model to learn and classify thermal images of the panels, thereby improving the stability of the solar system (Selvaraj et al., 2022). Recently, solar fault diagnosis technology has evolved an innovative global-local dual-stream collaborative framework for diagnosing multiple types of PV compound faults. This method involves constructing a shared CNN to extract fault features from both global and local streams, which enhances modeling efficiency and effectively verifies the actual fault locations on the PV panels (Liu et al., 2023).

These papers collectively highlight the critical role of advanced computational methods, including deep learning and artificial neural networks, in addressing the challenges of fault detection and diagnosis in solar PV systems. They underscore the importance of innovative techniques in ensuring the reliability, efficiency, and safety of solar energy as a key component of the global renewable energy portfolio.

This study focuses on developing a fault diagnosis platform for solar power systems, designed to effectively identify and diagnose potential faults within these systems. In terms of solar panel configuration, this research employs nine solar panels arranged in a three-series, three-parallel combination. By varying the number and configuration of solar panels in diverse experiments, the study aims to comprehensively investigate the performance of solar power systems and their behavior in response to faults. Regarding the performance metrics of the solar panels, under standard test conditions (STC), each solar panel boasts a maximum output power (P_{max}) of 20 W, cumulating in a total of 180 W. Under these conditions, the system's maximum power output voltage (V_{mp}) stands at 54.6 V, and the maximum power output current (I_{mp}) is 3.3 A. These performance metrics establish a baseline for subsequent fault diagnosis. For fault diagnosis, this study introduces a strategy that categorizes potential fault types into three detection methods: (i) PV system fault detection, (ii) PV panel dust accumulation detection, and (iii) PV array fault localization detection. Each method addresses different fault types and diagnostic requirements, ranging from the system level to the condition of individual solar panels, facilitating effective identification and analysis.

Table 1 shows a comparison of detection items for four PV system fault diagnosis strategies. The solar fault diagnosis method proposed in this study combines multiple regression analysis (MRA) and support vector machines (SVM) to effectively diagnose faults in PV panel surface dust accumulation, installation bracket failures, and related electrical equipment. This method demonstrates superior detection performance compared to the three strategies discussed in references (Alwar et al., 2022; Selvaraj et al., 2022; Liu et al., 2023). It is particularly suitable for areas with high air pollution and frequent earthquakes. This research is not limited to fault diagnosis of PV panels and electrical equipment but extends to a broader application scope, providing a comprehensive fault diagnosis solution.

In summary, this diagnostic platform not only enables the accurate identification of various fault types in solar power systems but also

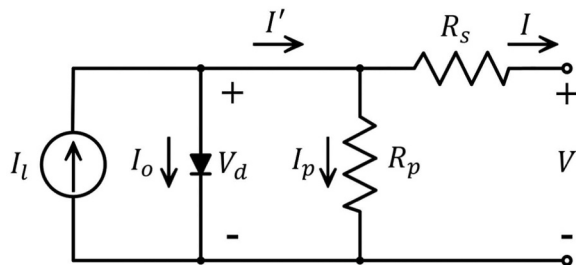


Fig. 1. Equivalent circuit of a solar cell.

provides effective fault localization, significantly boosting the operational efficiency and reliability of these systems. Moreover, the development of this diagnostic platform plays a crucial role in enhancing the practicality and economic viability of solar power technology, promoting its widespread adoption.

2. Introduction to solar photovoltaic systems

2.1. Electrical characteristics of solar cells

The equivalent circuit of a photovoltaic (PV) module can be described as a current source in parallel with an equivalent diode, as illustrated in Fig. 1. However, in practical applications, PV modules are influenced by series resistance (R_s) and shunt resistance (R_p). The series resistance (R_s) mainly consists of the internal resistance of the solar module, surface resistance, electrode conductivity resistance, and the contact resistance between the electrode and the silicon surface. On the other hand, the shunt resistance (R_p) primarily arises from contamination or inherent defects at the edges of the silicon wafer.

Through the equivalent circuit of the solar cell shown in Fig. 1, the relationship between the voltage (V) and current (I) of the solar cell can be derived using Kirchhoff's law, as shown in Eq. (1):

$$I = I_l - I_o \left[\exp \left(\frac{V + IR_s}{n \frac{kT_c}{q}} \right) - 1 \right] - \frac{V + IR_s}{R_p} \quad (1)$$

Where I_l represents the photocurrent; R_s is the series resistance; R_p stands for the shunt resistance; V denotes the output voltage; I indicates the output current; I_o is the reverse saturation current of the equivalent diode; n is the semiconductor ideal factor ($1 \leq n \leq 2$); k is the Boltzmann constant (1.38×10^{-23} J/K); and T_c is the temperature of the solar cell.

In the ideal state of a solar cell, Eq. (1) can be modified because the series resistance in the circuit is very small ($R_s \approx 0$) and can be neglected, while the shunt resistance is very large ($R_p \rightarrow \infty$), approaching an open circuit condition. Therefore, the equation can be simplified to Eq. (2):

$$I = I_l - I_o \left[\exp \left(\frac{V + IR_s}{n \frac{kT_c}{q}} \right) - 1 \right] \quad (2)$$

2.2. Types of photovoltaic system

2.2.1. Standalone photovoltaic system

A standalone photovoltaic (PV) system operates independently from the public grid, making it particularly suitable for remote areas, outdoor camping activities, ships, or situations where the public grid is unstable or unreliable. This type of system primarily consists of solar panels, batteries, direct current (DC) to alternating current (AC) inverters, and charge/discharge controllers. Solar panels are responsible for capturing solar radiation and converting it into electrical energy; batteries store

the electricity generated by the PV system for use during night time or poor weather conditions; inverters convert the direct current supplied by the batteries into alternating current; and controllers monitor the system's operational status and manage the charging and discharging of the batteries (Nirmal Mukundan et al., 2024).

Standalone PV systems offer several significant advantages: First, since they do not depend on the public grid, they can provide an independent power supply in remote or grid-unstable areas; second, as they do not need to connect to the public grid, their maintenance and upkeep are relatively simple; lastly, by eliminating the need for connection fees and electricity charges associated with the public grid, they can effectively reduce costs.

2.2.2. Hybrid photovoltaic system

Hybrid PV systems integrate solar power generation with other energy sources (such as wind power, diesel generators, etc.) to provide a more stable and reliable electricity supply, making them particularly suitable for scenarios with high power demand, such as villages, mining areas, and factories. The composition of such systems includes solar panels, batteries, DC/AC inverters, charge/discharge controllers, and rectifiers. Additionally, the system is equipped with supplementary energy devices such as wind turbines and diesel generators, also known as auxiliary generators. When the electricity output from the solar power generation is insufficient to meet user demands, the hybrid photovoltaic system automatically switches to other energy sources to ensure power supply (Sun et al., 2024).

The advantages of hybrid PV systems include stability and reliability: by combining multiple energy sources like solar, wind, and diesel, the hybrid system can automatically switch between sources based on actual needs, ensuring a stable and reliable electricity supply. Cost-effectiveness: through design and configuration tailored to local conditions, hybrid systems make full use of renewable energies such as solar and wind power, helping to reduce fuel costs and thereby lowering overall operational costs. Easy to expand: as electricity demand increases, the hybrid system can be easily expanded, for example, by adding more solar panels, energy storage batteries, or wind turbines to accommodate greater power needs.

2.2.3. Grid-tied PV system

The grid-tied PV system is an advanced solution that closely connects the solar power generation system with the public power grid (also known as the electric power grid). With the help of an inverter, solar power is converted into alternating current that can be used by the grid and then fed into the public grid. This system not only allows the solar power generation system to be self-sufficient but also enables the sale of surplus electricity to the public grid, implementing bidirectional metering to optimize energy efficiency. Its architecture includes key components such as solar panels, direct current (DC) to alternating current (AC) inverters, and AC electricity meters. Solar panels are responsible for converting solar energy into DC, which is then converted into AC by the inverter. The AC electricity meter accurately measures the amount of electricity generated and consumed, ensuring seamless coordination between the solar PV system and the public grid (Magableh et al., 2024).

The grid-tied PV system exhibits the following significant advantages: self-sufficiency, able to meet the electricity needs of individual households while selling surplus electricity to the public grid through bidirectional metering, further saving on electricity costs. Moreover, by optimizing power distribution, the system effectively reduces energy consumption, and because it does not require additional energy storage devices, it significantly simplifies system maintenance and management, enhancing the user experience.

3. The proposed solar power generation platform architecture

The solar power generation system platform in this study mainly

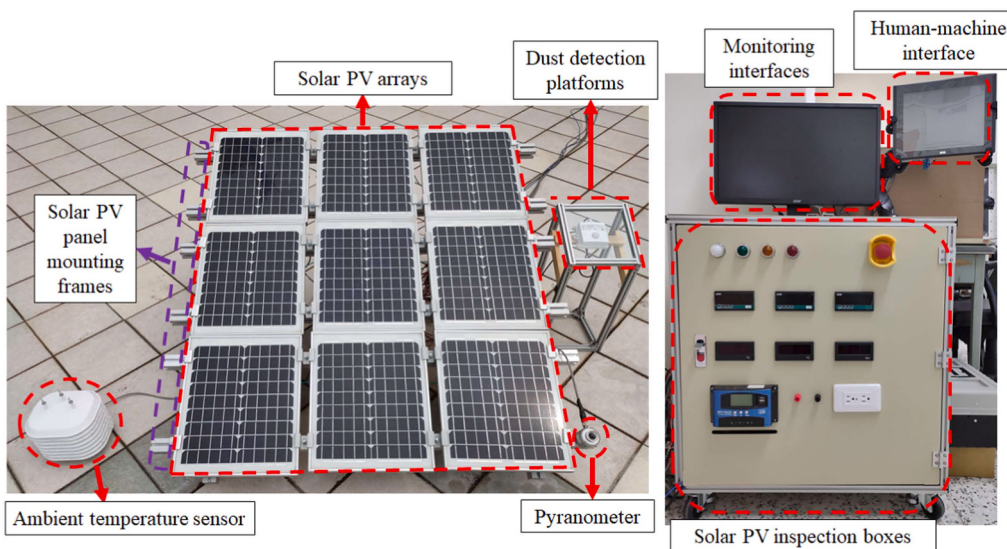


Fig. 2. Physical diagram of the solar power generation system platform.

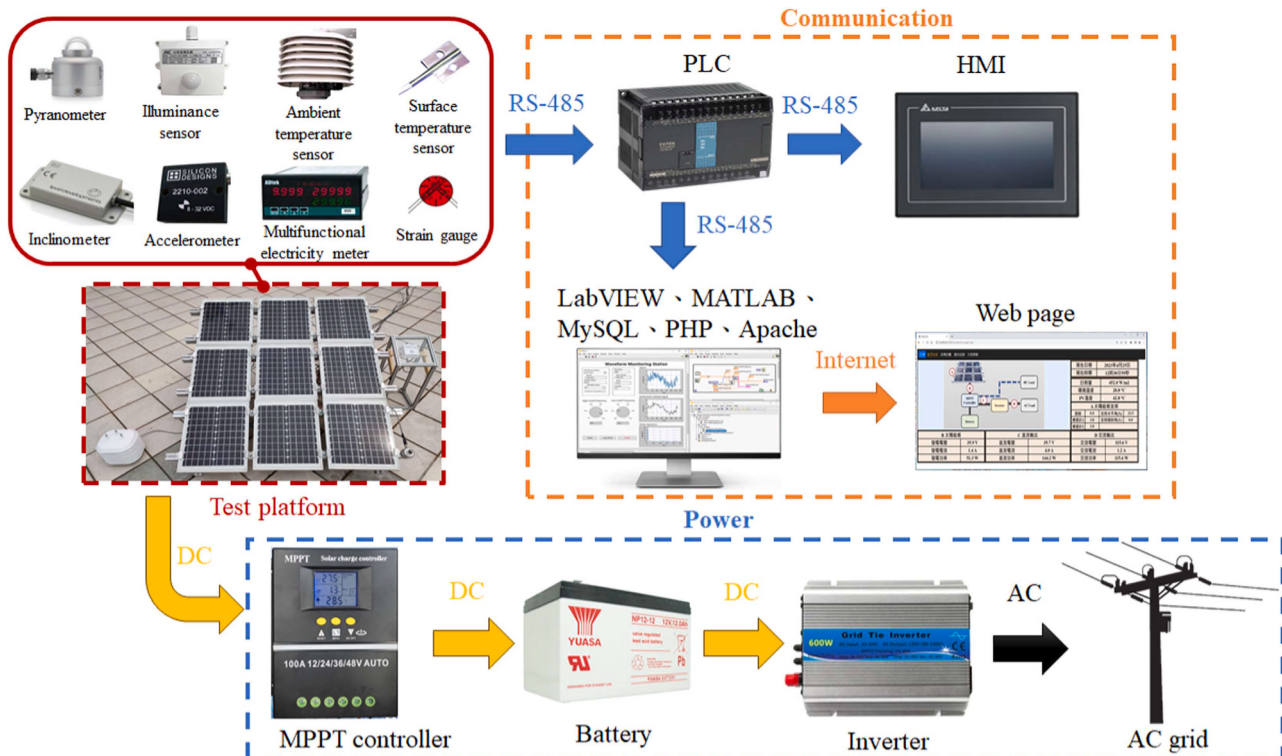


Fig. 3. Diagram of the solar power generation platform structure.

comprises solar photovoltaic (PV) arrays, solar PV panel mounting frames, dust detection platforms, solar PV inspection boxes, monitoring interfaces, etc., as depicted in Fig. 2. A total of 9 solar PV panels were utilized in this study, with the primary system configuration being three in series and three in parallel. Different numbers of panels and configurations will be employed for experiments. Under standard test conditions (STC), a single solar panel was determined to have a maximum output power (P_{max}) of 20 W, a maximum open-circuit voltage (V_{oc}) of 22.4 V, a maximum short-circuit current (I_{sc}) of 1.19 A, a maximum power output voltage (V_{mp}) of 18.2 V, and a maximum power output current (I_{mp}) of 1.1 A. Consequently, the total P_{max} of all solar panels combined is 180 W, with a V_{mp} of 54.6 V and a I_{mp} of 3.3 A.

This study examines the structure of a solar power generation system as illustrated in Fig. 3, which consists of both electrical and communication components at its core. Electrically, the system harnesses energy through a PV array and employs a maximum power point tracking (MPPT) controller to efficiently store this generated energy in batteries. The stored energy is subsequently converted by an inverter to power the grid. In terms of communication, the architecture primarily utilizes a programmable logic controller (PLC) to gather data from various sensors installed on the experimental platform via the RS-485 interface and analog signal transmission methods. These sensors include a pyranometer, illuminance sensor, solar panel surface temperature sensor, ambient temperature sensor, inclinometer, accelerometer, strain gauge,



Fig. 4. Physical diagram of sensor elements installed on the solar panel mounting bracket.



Fig. 5. Dust detection platform.

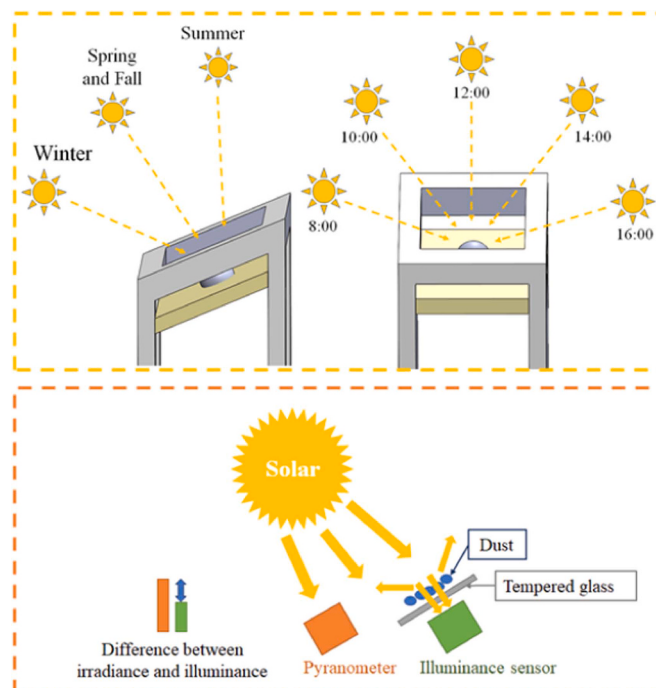


Fig. 6. Design of light sensing in response to changes in sunlight.

as well as sensors for solar panel power generation, DC transmission, and AC grid supply data. The collected data undergoes initial processing by the PLC before being transmitted to the on-site human-machine

interface (HMI) and personal computer (PC) through RS-485, where it is further analyzed and processed using the graphical programming software, LabVIEW. The HMI is chiefly responsible for real-time monitoring and fault diagnostics, whereas LabVIEW software is dedicated to advancing data analysis, storage, and network transmission. Data analysis leverages mathematical equations formulated in Laboratory Virtual Instrumentation Engineering Workbench (LabVIEW) and is further enhanced with MATLAB software. Data storage is facilitated by the PC's hard drive and a My Structured Query Language (MySQL) database. The integration of MySQL, Hypertext Preprocessor (PHP), and Apache enables a dynamic web page, equipping the entire system with Internet of Things (IoT) functionality and completing an extensive solar photovoltaic system.

3.1. Explanation of sensor elements

In this study, we installed various sensor elements on the mounting brackets of the solar panels, as illustrated in Fig. 4, including inclinometers, accelerometers, and strain gauges. By installing inclinometers, we primarily measure the tilt angle of the brackets on the horizontal plane to assess whether the foundation of the mounting system has been compromised due to environmental factors or natural disasters, thereby affecting the efficiency and power generation of the solar panels. The purpose of the accelerometers is to monitor the vibration of the mounting system to determine if there are any loose screws. Loose screws can be caused by environmental corrosion leading to rust, or due to being overtightened during installation, which damages the threads and causes them to loosen. By measuring the vibration of the mounting system, we can promptly identify and address these potential issues. Furthermore, the installation of strain gauges is intended to measure the stress and deformation the mounting system endures during use. Especially at the junctions where the solar panel mounting brackets support aluminum crossbeams and elevation stands, these areas are prone to weakening due to the weight of the solar panels and the external forces of nature such as wind and snow, leading to bending or twisting of the mounting system. Regular measurement and monitoring of the strain gauge data help ensure the safety and reliability of the solar panel mounting system, enabling timely maintenance or replacement as necessary.

3.2. Explanation of light sensing

To delve into the impact of dust on the efficiency of solar panel electricity generation, this study has developed a dust detection platform, utilizing light sensors to analyze the effects of dust, as shown in Fig. 5. This platform enables us to specifically analyze how dust affects

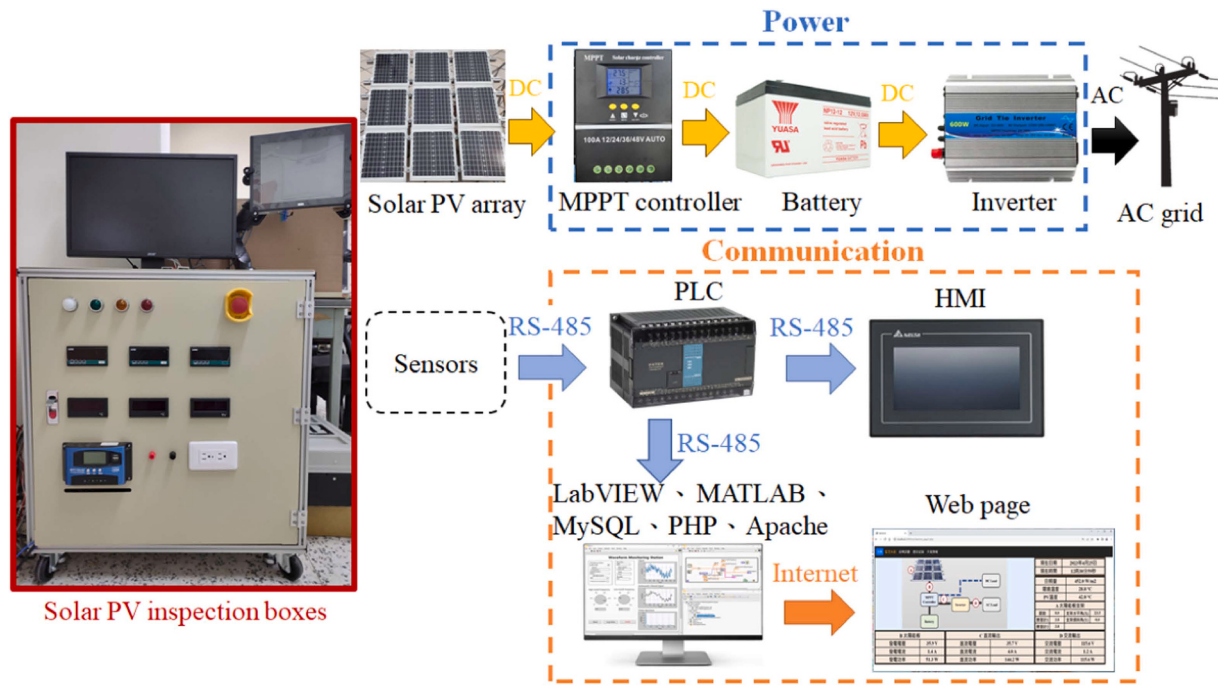


Fig. 7. Structure of solar PV testing box.

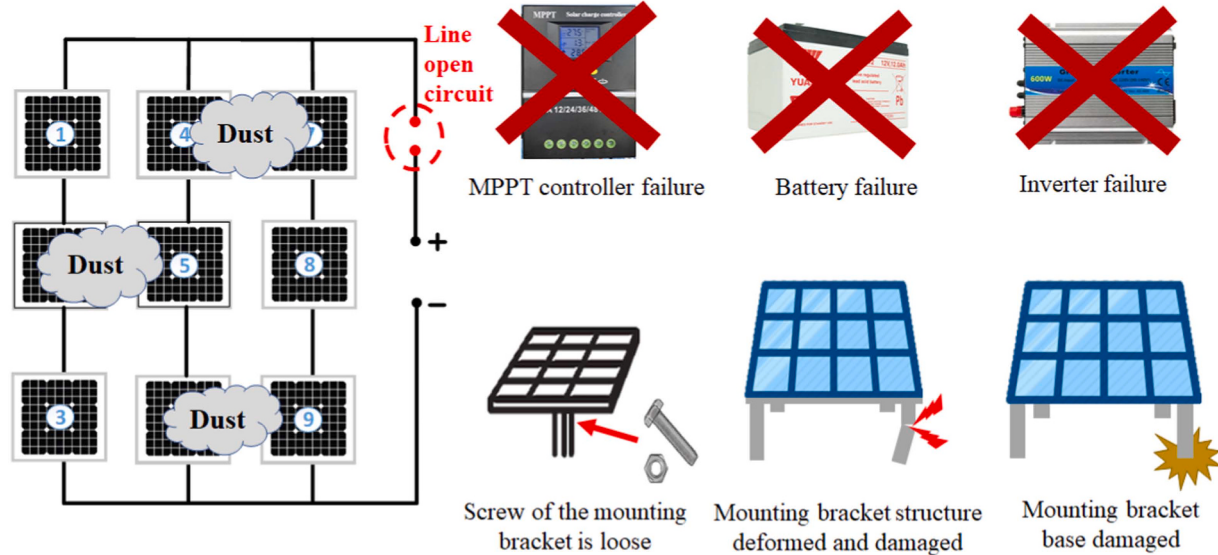


Fig. 8. Setting of PV system fault points.

the efficiency of solar energy generation, thereby assessing the cleanliness of solar panels to further enhance their power generation efficiency. The operating principle of the dust detection platform is based on light sensors measuring the sunlight that has been attenuated by passing through tempered glass and its surface dust. These measurements are compared with those from a pyranometer to calculate the amount of dust on the tempered glass surface, estimating the impact of dust on the efficiency of solar panel power generation. The reason for choosing tempered glass is that it shares the same material properties as the glass used in solar panels, achieving the same level of light transmission. The dimensions of the glass were designed considering the varying angles of sunlight from morning to evening and across different seasons, as illustrated in Fig. 6. Light sensors can finely capture minute changes in light intensity and offer the advantage of being cost-effective. By using

light sensors in conjunction with a pyranometer, we can measure changes in light intensity caused by dust under the same sunlight conditions, thereby accurately assessing the impact of dust.

3.3. Explanation of solar PV testing box

The solar PV testing box constructed in this study features two main functionalities, as demonstrated in Fig. 7. Firstly, the energy section includes both standalone and grid-tied system configurations. The standalone system utilizes a maximum power point tracking (MPPT) controller to maximize power output from the solar PV modules, subsequently storing this energy in batteries and supplying it to loads through an inverter. In contrast, the grid-tied system refers to the setup where the electricity generated by the solar PV modules is connected to

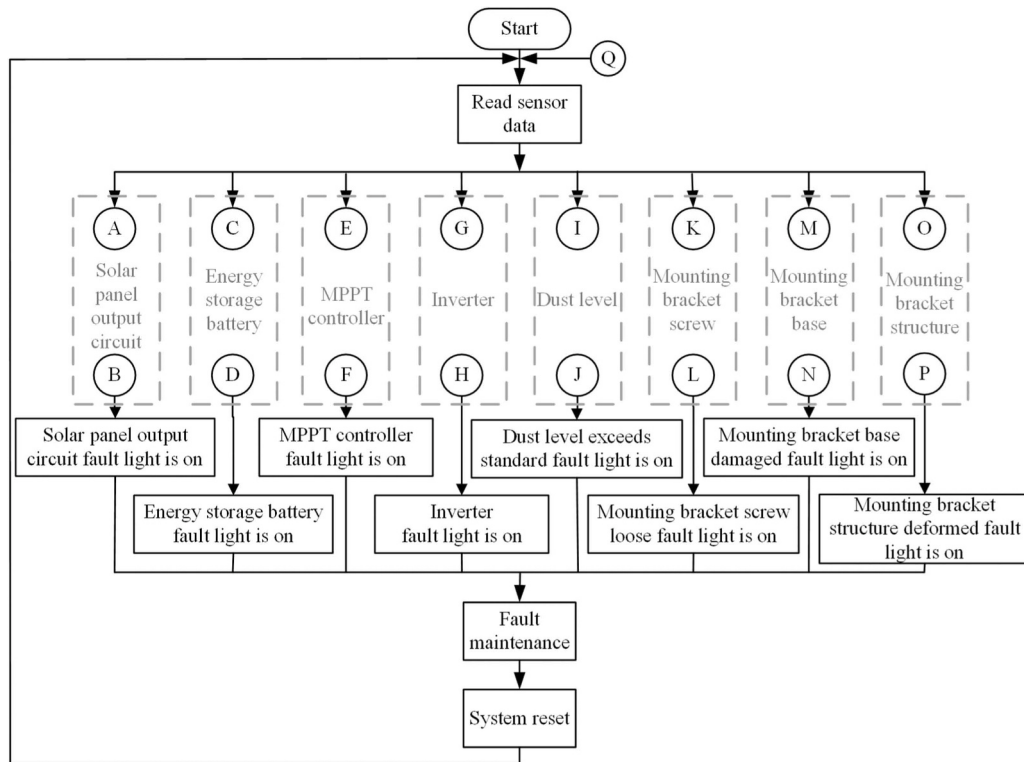


Fig. 9. Flowchart for solar PV system fault detection.

the public grid via an inverter. Secondly, the communication section collects signals from various sensors through a PLC and conducts preliminary processing of these signals. These signals are then transmitted to the HMI monitoring screen and computer via the RS485 communication protocol. On the computer, the signals are further analyzed using LabVIEW and MATLAB software. Additionally, by integrating MySQL, Apache, and PHP technologies to create dynamic web pages, not only can data be stored, but it can also be analyzed and displayed, thereby enabling comprehensive management and application of solar PV testing data.

4. The proposed fault diagnosis strategy

4.1. Fault patterns in this study's solar energy system

The types of faults in the solar PV system in this study include issues with the inverter, MPPT controller, energy storage batteries, output circuitry of the solar panels, excessive dust, loosening of the mounting bracket screws, damage to the foundation of the mounting bracket, and structural deformation of the bracket, as detailed in Fig. 8. A common fault in inverters and MPPT controllers involves damage to the switch mechanism. Energy storage batteries might face challenges like inadequate charging, insufficient discharge, or diminishing capacity, potentially rendering them inoperable. The output circuitry of solar panels could degrade, leading to loosening or fracture if it remains exposed to external conditions for a long time. The accumulation of dust can notably diminish the power generation efficiency of solar panels. Additionally, screws on the mounting brackets are susceptible to rusting or deforming, potentially loosening over time due to prolonged exposure to environmental elements. Moreover, the mounting brackets may suffer alterations in angle, material, and structure as a result of natural disasters such as landslides or subsidence. Hence, conducting regular inspections and maintenance of the system is essential to prevent faults and damage.

4.2. Fault diagnosis strategy of this study

This study categorizes fault types into three detection strategies, including: (i) solar PV system fault detection, (ii) solar panel dust accumulation detection, and (iii) fault localization detection for solar PV arrays. The following sections will provide a detailed introduction to these strategies.

4.2.1. Solar PV system fault detection

Fault detection within the solar PV system covers eight primary categories, including output circuitry of the solar panels (points A and B), energy storage batteries (points C and D), MPPT controllers (points E and F), inverters (points G and H), dust accumulation (points I and J), loosening of the mounting bracket screws (points K and L), damage to the mounting bracket foundation (points M and N), and deformation or damage to the mounting bracket structure (points O and P). The detection procedure entails identifying faults by analyzing sensor data. If no fault is identified (point Q), the system will resume sensor data collection. When a fault is detected, an indicator light will activate, signaling maintenance personnel to carry out fault repair. After the fault has been rectified, the system reverts to collecting sensor data. Please see Fig. 9 for a comprehensive flowchart of the solar photovoltaic system fault detection process.

4.2.1.1. The fault diagnosis mechanism of the output circuitry of the solar panels (points A and B).

Solar panels transmit electrical energy from the solar PV array to the MPPT controller via the output circuitry. If the output circuitry of the solar panels is interrupted due to external factors, the generated electrical energy cannot be transmitted to the back-end of the system, leading to energy loss and potential disasters. When the pyranometer measures sunlight intensity exceeding 50 W/m^2 , sufficient to power the solar panels, and the electricity voltage measured under the influence of an open circuit at the solar array's output end by the MPPT controller and energy storage battery is between 3.3 V to 3.6 V, a criterion is set: if the lowest voltage value exceeds 5 V, it is determined that

there is a break or open circuit in the solar panel's output circuitry, necessitating fault diagnosis and remediation.

4.2.1.2. The fault diagnosis mechanism of the energy storage batteries (points C and D). Energy storage batteries are batteries that can store electrical energy and release it when needed. If it is determined that the energy storage battery is disconnected from the system or damaged and cannot continue to be used, causing the photovoltaic array to be unable to supply power to the energy storage battery and the backend system, immediate maintenance must be carried out to ensure the normal operation of the system. When the generating electricity meter measures that the voltage of the photovoltaic array is greater than 5 V and the current is less than 0.1 A, and the voltage meter at the energy storage battery end cannot measure within the normal range (36 V to 54.6 V) ([Taiwan Yuasa battery, 2024](#)), it will be determined that the energy storage battery is disconnected from the system or damaged.

4.2.1.3. The fault diagnosis mechanism of the MPPT controllers (points E and F). The maximum power point tracking (MPPT) controller is a device designed to enhance the efficiency of solar panels. A malfunctioning MPPT controller can hinder the solar panels from operating at their optimal power point, thereby diminishing the efficiency of electricity generation. Thus, when the voltage of the solar panels exceeds 5 V and the current is below 0.1 A, while the voltage at the energy storage battery end remains within the normal range (36 V to 54.6 V) ([Taiwan Yuasa battery, 2024](#)), it could indicate a malfunction in the MPPT controller. Should component damage that prevents normal operation be identified, immediate replacement or repair is recommended.

4.2.1.4. The fault diagnosis mechanism of the inverters (points G and H). The inverter is a device that converts DC into AC, facilitating the conversion of DC output from solar panels into AC electricity for residential, commercial, or industrial use. Ensuring the inverter's proper functioning is crucial for the continuous supply of electricity to the load end and for maintaining system operation. Initially, the voltage at the battery terminal should be measured to verify an adequate power supply to the inverter. It is also important to check whether a load is connected and if it is in an open state. If these conditions are met satisfactorily, the output current of the inverter must be measured. A lack of output current signals a fault with the inverter, requiring immediate replacement or repair.

4.2.1.5. The fault diagnosis mechanism of the dust accumulation (points I and J). The accumulation of dust on solar panels negatively impacts their power generation efficiency. If the power output of a solar panel array drops below 80 % of the predicted value ([Anon, 2024a](#)), it is considered that excessive dust has accumulated, necessitating cleaning.

4.2.1.6. The fault diagnosis mechanism of the loosening of the mounting bracket screws (points K and L). Solar panels are mounted on fixed brackets. Should the screws on these brackets become loose, the panels might sway or shift, negatively impacting the system's power generation efficiency. To determine the tightness of the screws, we measure vibration data using an accelerometer and assess the panels' tilt with an inclinometer. Research indicates that the optimal angle for solar panels in Taichung, Taiwan, is 23.5 degrees ([Anon, 2024b](#)). If the inclinometer reads 23.5 degrees on the Y-axis and 0 degrees on the X-axis, but the accelerometer's vibration data exceeds ± 0.5 g, it suggests that the screws may be loose.

4.2.1.7. The fault diagnosis mechanism of the damage to the mounting bracket foundation (points M and N). The foundation of the fixed bracket supports the weight of the solar panels as well as withstands the external forces of wind and rain. Damage to this foundation can significantly impair the stable operation of the solar energy system. To assess the

condition of the foundation, we use an inclinometer to measure its angle. If the inclinometer readings deviate from 23.5 degrees on the Y-axis or 0 degrees on the X-axis, it indicates that the foundation of the fixed bracket may be compromised.

4.2.1.8. The fault diagnosis mechanism of the deformation or damage to the mounting bracket structure (points O and P). Deformation within the fixed bracket structure typically occurs at the bracket joints, the most susceptible areas to damage. To detect any deformation, strain gauges are installed at these joints, with data subsequently collected for analysis. Considering the thermal expansion and contraction characteristics of aluminum, its expansion coefficient (α) is $23.1 \times 10^{-6}/^\circ\text{C}$. In Taichung, Taiwan, where temperatures generally fluctuate between 20 °C and 40 °C, this results in a temperature differential (ΔT) of 20 °C. Assuming an aluminum component length (L) of 0.5 m, the strain (ϵ) induced by thermal expansion can be calculated using the formula for strain, resulting in a variation of 231 $\mu\text{m/m}$. With an installation temperature of 30 °C, the effective strain range is determined to be from $-115.5 \mu\text{m/m}$ to $115.5 \mu\text{m/m}$. Deviations beyond this range indicate that the fixed bracket structure has experienced deformation.

$$\epsilon = \alpha \times \Delta T \times L \quad (3)$$

4.2.2. Detection of dust accumulation on solar panels

This study explores methods for detecting dust accumulation on solar panels, assesses the impact of dust on power generation through the use of cost-effective light sensors, and details both linear regression techniques and dust detection methods. With the growing prevalence of solar panels in daily life, the issue of surface dust accumulation has become increasingly significant. Such accumulation not only diminishes the efficiency of solar power systems but may also result in equipment malfunctions or damage. Consequently, it is vital to develop an efficient method for detecting dust accumulation on solar panels.

4.2.2.1. Introduction to linear regression. This study employed two types of linear regression analysis methods. Initially, when the analysis involves only one independent variable and one dependent variable, we utilize simple linear regression (SLR) ([JMP Statistical Discovery LLC, 2024](#)). Subsequently, in cases where the relationship between multiple predictor variables and a single dependent variable is analyzed, we employ multiple regression analysis (MRA) ([Multiple linear regression analysis, 2024](#)).

The SLR model is designed to calculate the relationship between an independent variable and a dependent variable, constructed using only one independent variable (x) and one dependent variable (y). For instance, Eq. (4) illustrates the equation of SLR, where β_0 represents the intercept, and β_1 serves as the slope, indicating the change in y for a one-unit change in x . The primary goal of the analysis, or the so-called Loss Function, aims to find a set of parameters (β_1 and β_0) that minimize the model's residual values

$$y = \beta_1 x + \beta_0 \quad (4)$$

The parameters β_1 and β_0 can be determined through the least square method (LAM) ([Least squares method, 2024](#)). The primary purpose of this method is to find the parameter values that minimize the square of the error. The reason for squaring is that error values can be positive or negative, and squaring them ensures they are all positive values. Therefore, the objective is to make the sum square error (SSE) for all training samples as close to 0 as possible, as shown in Eq. (5):

$$\text{Loss}(\widehat{\beta_0}, \widehat{\beta_1}) = \sum_{i=1}^n (y_i - \widehat{y}_i)^2 = \sum_{i=1}^n (y_i - (\widehat{\beta_0} + \widehat{\beta_1}x_i))^2 \quad (5)$$

To derive β_0 , it is necessary to perform a partial derivative of the loss function (β_0, β_1) with respect to β_0 and set it equal to zero, as shown in Eq. (6):

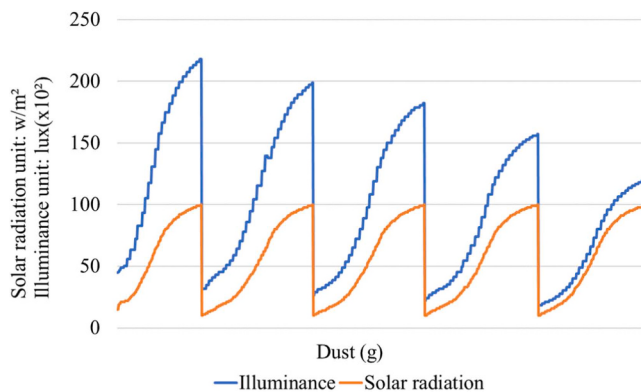


Fig. 10. Comparison chart of the effects of dust on illuminance and solar radiation.

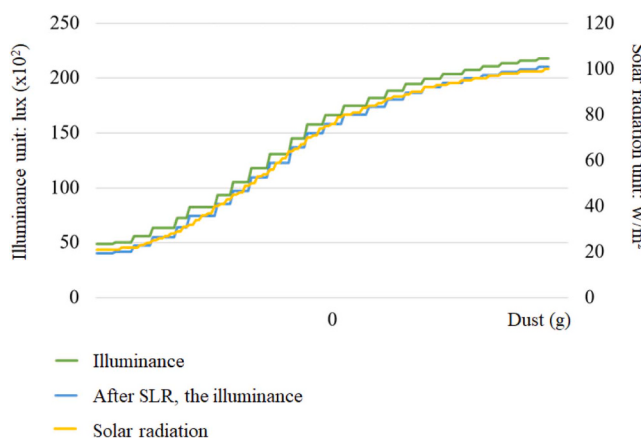


Fig. 11. Illuminance curve chart after SLR.

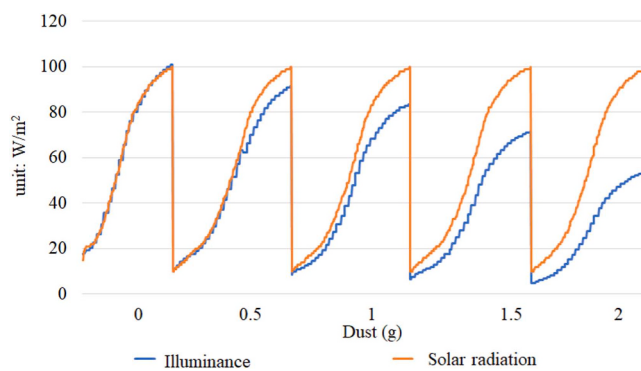


Fig. 12. Curve chart of the effects of various dust concentrations after SLR.

$$\frac{\partial \text{Loss}(\hat{\beta}_0, \hat{\beta}_1)}{\partial \beta_0} = \frac{\partial \sum_{i=1}^n (y_i - \hat{\beta}_0 + \hat{\beta}_1 x_i)^2}{\partial \beta_0} = 0$$

$$\Rightarrow \hat{\beta}_0 = \bar{y} - \hat{\beta}_1 \bar{x} \quad (6)$$

To derive β_1 , it is necessary to perform a partial derivative of the loss function (β_0, β_1) with respect to β_1 and set it equal to zero, as shown in Eq. (7):

$$\frac{\partial \text{Loss}(\hat{\beta}_0, \hat{\beta}_1)}{\partial \beta_1} = \frac{\partial \sum_{i=1}^n (y_i - \hat{\beta}_0 + \hat{\beta}_1 x_i)^2}{\partial \beta_1} = 0$$

$$\Rightarrow \hat{\beta}_1 = \frac{\sum_{i=1}^n (y_i - \bar{y})(x_i - \bar{x})}{\sum_{i=1}^n (x_i - \bar{x})^2} \quad (7)$$

In the equation, \bar{x} and \bar{y} represent the mean values of x and y , respectively. By applying the formula derived from the aforementioned least squares method, it is possible to solve for the parameters β_1 and β_0 . Substituting these parameters into the simple linear regression (SLR) equation allows for the construction of a complete SLR model.

Additionally, multiple regression analysis (MRA) aims to explore the interrelationships between multiple predictor variables (independent variables) and a single dependent variable. In this analysis, the dependent variable needs to be a continuous variable. The mathematical model for multiple linear regression can be represented as Eq. (8), where the regression coefficients $\beta_1, \beta_2, \dots, \beta_k$, and x_1, x_2, \dots, x_k represent the predictive power of k variables on y , β_0 is the regression model intercept, and ϵ is the error term.

$$y = \beta_1 x_1 + \beta_2 x_2 + \dots + \beta_k x_k + \beta_0 + \epsilon \quad (8)$$

Essentially, MRA is similar to SLR analysis, with the primary difference being the inclusion of more independent variables. Assuming there are n pieces of data, d independent variables, and one dependent variable, the regression equation in this context can be represented in matrix form as Eq. (9), while also calculating the Loss (β) value of the loss function. This process is similar to subsequent steps in SLR analysis, requiring the estimation of β values. By setting the partial derivative with respect to β equal to zero to find the optimal solution, the coefficients of the multiple regression line are obtained. Just like univariate linear regression, this method can provide an analytical solution.

$$Y_{n \times 1} = X_{n \times (d+1)} \beta_{(d+1) \times 1}$$

$$Y = \begin{bmatrix} y_1 \\ y_2 \\ \vdots \\ y_n \end{bmatrix}_{n \times 1}, \beta = \begin{bmatrix} \beta_1 \\ \beta_2 \\ \vdots \\ \beta_d \end{bmatrix}_{(d+1) \times 1}$$

$$X = \begin{bmatrix} X_1^T \\ X_2^T \\ \vdots \\ X_n^T \end{bmatrix} = \begin{bmatrix} 1 & x_1^{(1)} & \dots & x_1^{(d)} \\ 1 & x_2^{(1)} & \dots & x_2^{(d)} \\ \vdots & \vdots & \ddots & \vdots \\ 1 & x_n^{(1)} & \dots & x_n^{(d)} \end{bmatrix}_{n \times (d+1)} \quad (9)$$

4.2.2.2. Based on the dust detection method. In this experiment, we simulated real-world dust using flour and employed a cost-effective light sensor to detect the impact of dust. The experiment measured the sunlight intensity recorded by a pyranometer (in units of W/m^2) and the illuminance received by a light sensor placed under tempered glass (in units of Lux), using the difference between these measurements as a basis for quantifying dust levels. The results demonstrated that, under the same sunlight intensity conditions, different concentrations of dust significantly affected the illuminance received by the light sensor, as shown in Fig. 10. Through this experiment, we gained a deeper understanding of the impact of dust on light intensity and showcased how to measure dust concentrations using an affordable light sensor.

To enhance the accuracy of the experimental results and the clarity of observations, this study utilized simple linear regression (SLR) analysis to adjust the parameters of illuminance (in units of Lux) and solar radiation (in units of W/m^2) to equivalent physical quantities. This adjustment made the subsequent mathematical computations more convenient. The SLR equation between illuminance (x_i) and solar radiation (y_s) is defined as Equation (10). After the SLR analysis, a curve expressed in equivalent physical quantities was obtained, as shown in

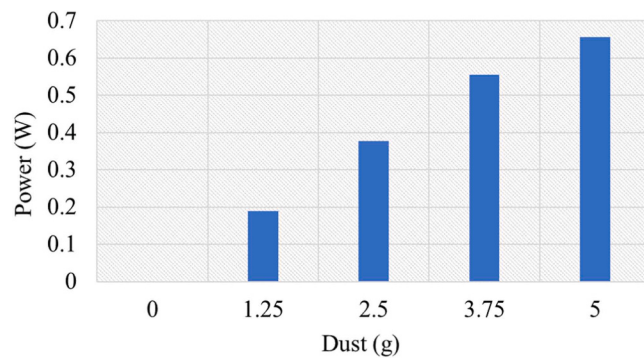


Fig. 13. Power loss chart due to dust accumulation.

Fig. 11. Further, the adjusted data revealed the relationship between illuminance and solar radiation under different dust concentrations, as illustrated in **Fig. 12**.

To investigate the impact of dust on the power generation efficiency of solar PV panels, this study conducted an empirical experiment by

measuring the relationship between solar radiation and illuminance. The experiment utilized a piece of tempered glass and a single solar PV panel, both with an effective area ratio of 1:2.5. Different amounts of flour were evenly spread on the tempered glass and the solar panel to simulate the accumulation of dust, with the dust quantity ranging from 0 g to 2 g on the tempered glass, changing by 0.5 g increments, and from 0 g to 5 g on the solar PV panel, changing by 1.25 g increments. The experiments were conducted under solar radiation conditions of 100 W/m^2 on the single solar PV panel, with five repeated trials for the same amount of dust and the average value calculated. The experimental results showed that the power generation capacity of the solar panel was affected to varying degrees with the increase of dust quantity, as detailed in **Fig. 13**.

Based on the experimental results presented in **Fig. 13**, we observed that accumulations of dust of varying degrees have significantly different impacts on the power generation efficiency of solar PV panels. To accurately calculate power loss, we first measured the power generation of solar PV panels without any dust coverage and then recorded the power generation of the panels affected by different amounts of dust coverage, thereby calculating the power differential caused by dust accumulation.

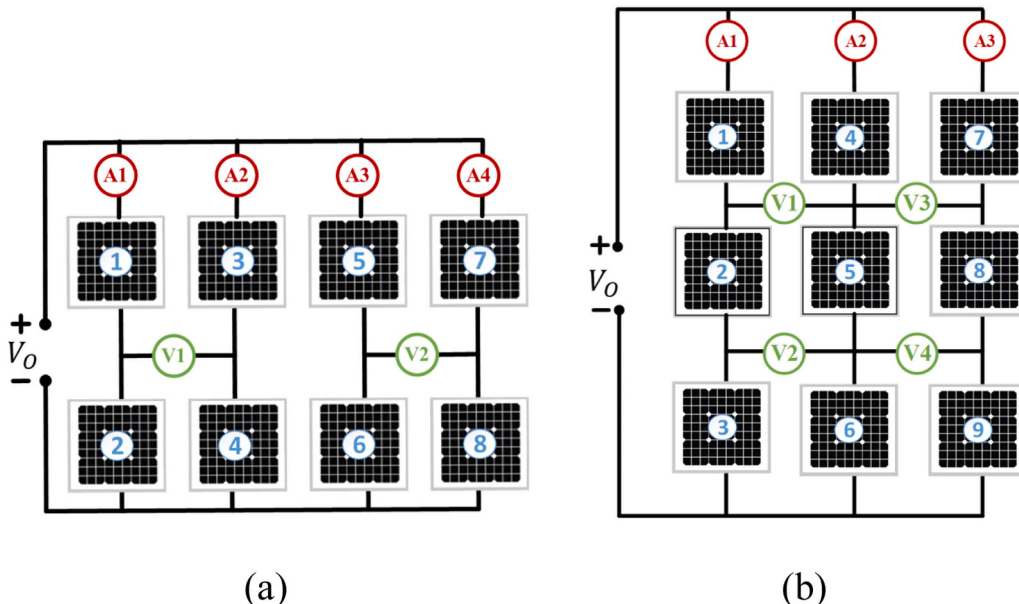


Fig. 14. The arrangement of the solar PV array and the installation positions of the voltmeter and ammeter: (a) 2 in series and 4 in parallel, (b) 3 in series and 3 in parallel.

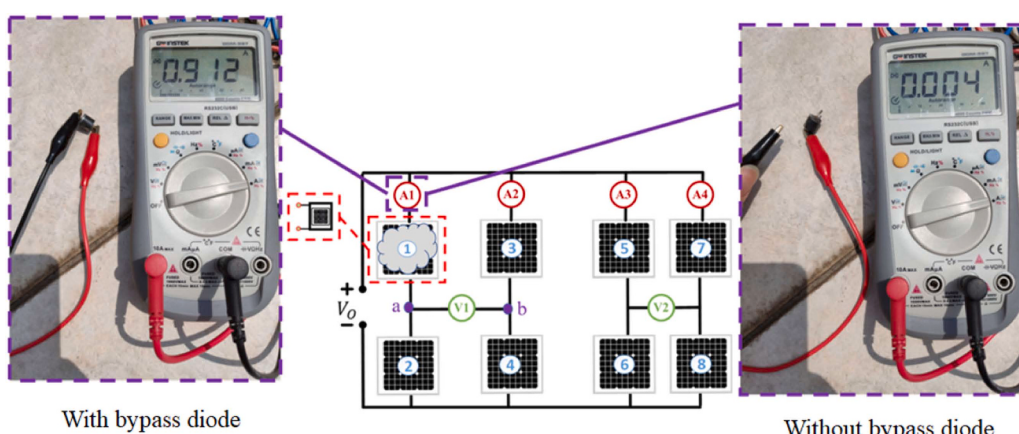


Fig. 15. Schematic diagram illustrating the interruption of current due to an open circuit fault in the bypass diode of PV panel (1).

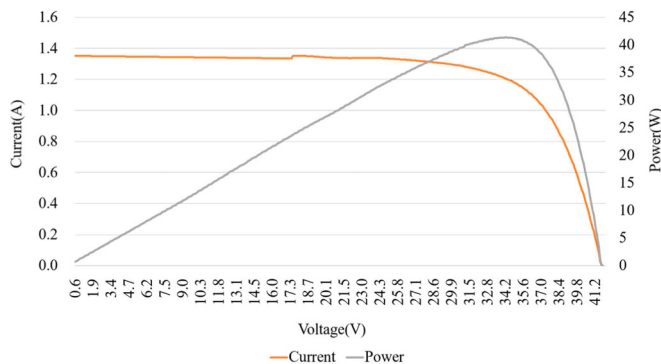


Fig. 16. The I-V characteristic curve of a PV panel under conditions of 300 W/m² solar irradiance and a temperature of 25°C.

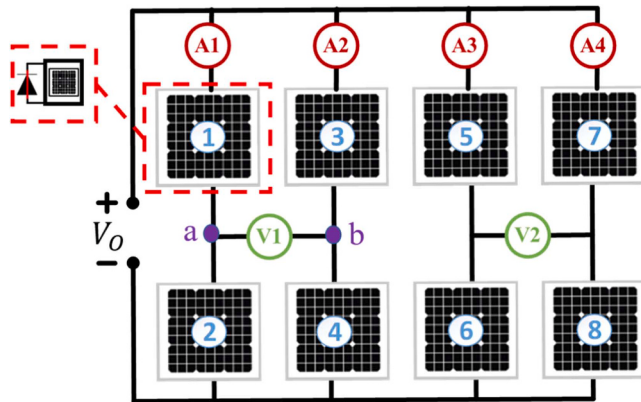


Fig. 17. Schematic diagram showing a bypass diode short-circuit fault in PV panel (1).

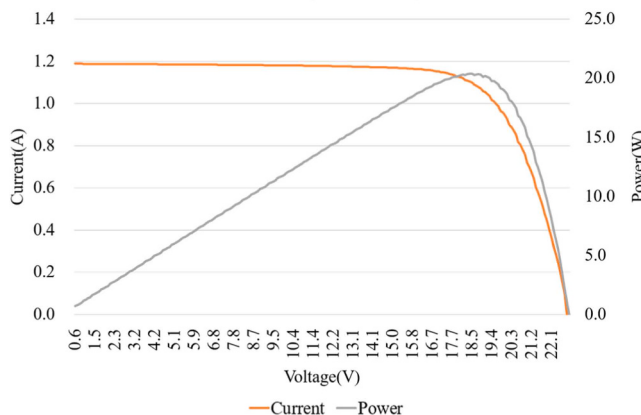


Fig. 18. The I-V characteristic curve of PV panel (1) with a bypass diode short-circuit fault, under conditions of 300 W/m² solar irradiance and a temperature of 25 °C.

To estimate the impact of dust on the power generation efficiency of solar photovoltaic (PV) panel arrays solely based on solar radiation (x_1) and illuminance (x_2), this study employed multiple regression analysis (MRA) to estimate the power loss caused by dust accumulation on solar PV panels. The predictive formula for power loss is defined as Eq. (11):

$$P_L = -8.1679x_1 - 15.1453x_2 + 0.0022415x_1^2 + 0.004788x_1x_2 + 0.005821x_2^2 + 10572.996 \quad (11)$$

In order to accurately determine whether the decrease in power

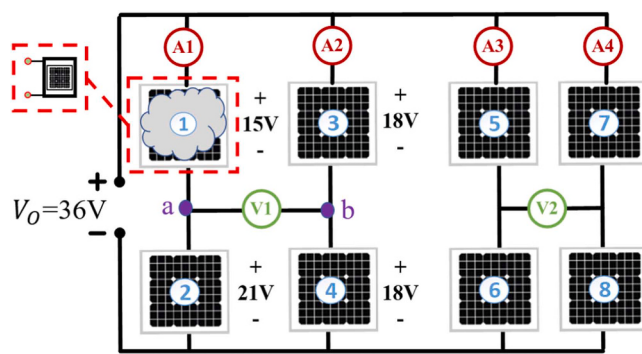


Fig. 19. Schematic diagram showing a bypass diode open-circuit fault in PV panel (1).

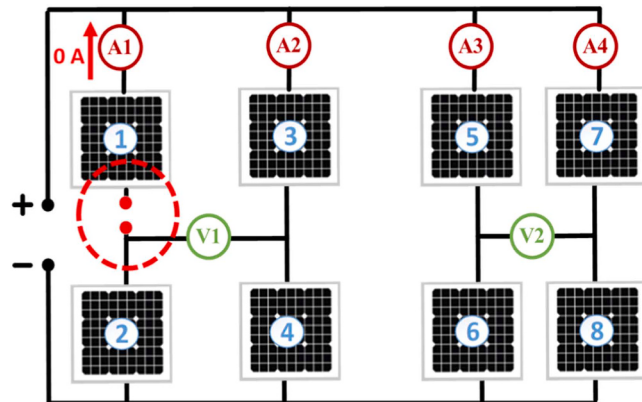


Fig. 20. Downstream circuit open fault in PV panel (1).

generation of the solar PV system is due to dust accumulation or other faults causing the decrease in electricity generation, we have added the solar photovoltaic power generation prediction Eq. (12) and the equation for power loss due to dust influence (13):

$$P_o = P_{ref} \times m \times (1 - \gamma \times (T - T_{ref})) \times \left(\frac{I}{I_{ref}} \right) + K \quad (12)$$

Where P_o is the predicted power generation of the solar PV array; P_{ref} is the power generation of a single solar PV panel under standard test conditions; m is the number of solar panels; γ is the temperature coefficient (0.37 %/°C); T is the measured temperature of the solar PV panels; T_{ref} is the temperature of the solar PV panels under STC (25 °C); I is the measured solar radiation; I_{ref} is the solar radiation under STC (1000 W/m²); K is the calibration factor.

$$P_d = P_{ref} \times m \times (1 - \gamma \times (T - T_{ref})) \times \left(\frac{I}{I_{ref}} \right) - P_L + K \quad (13)$$

Where P_d is the predicted power generation of the solar PV array based on dust effects; P_L is the power loss (dust influence).

According to Eqs. (12) and (13), by observing the relationship between the actual power generation (P), the predicted power generation of the solar PV array (P_o), and the predicted power generation of the solar PV array based on dust effects (P_d), the reasons for power reduction are evaluated. When P , P_o , and P_d are close to each other, it indicates that the system is not affected by dust and no malfunction has occurred. When P deviates from P_o and P_d , it indicates a system malfunction. When P is close to P_d and deviates from P_o , it indicates a reduction in power generation due to dust effects.

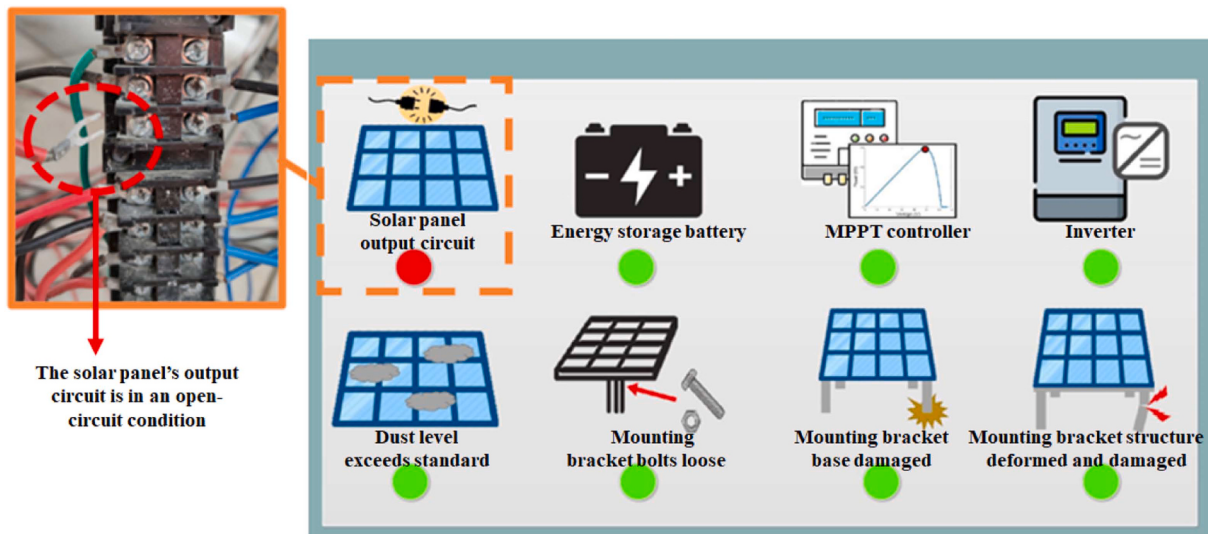


Fig. 21. The system platform fault diagnosis displays a solar PV panel output circuit fault.

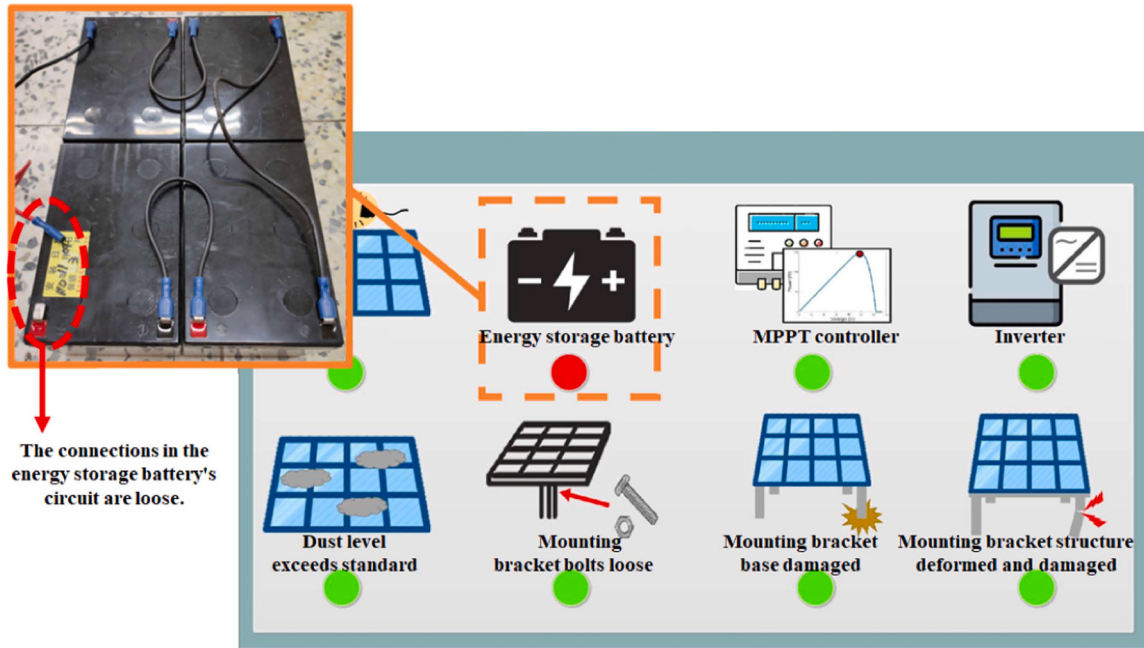


Fig. 22. The system platform fault diagnosis displays an energy storage battery fault.

4.2.3. Solar PV array fault localization detection method

The fault detection method for solar PV arrays encompasses three components: diode short circuit, diode open circuit, and line open circuit. Faults such as diode short circuits and diode open circuits within the solar PV panel can be pinpointed by measuring the fault voltage. To facilitate automated fault localization, a support vector machine (SVM) can be employed to ascertain the fault's location. Moreover, ammeters installed within the solar PV array are capable of detecting open circuit faults through the measurement of current data, enabling the precise identification of fault locations in the solar PV panels.

4.2.3.1. Introduction of the support vector machine. In the fault localization detection method for solar photovoltaic arrays, this study employed the fitcecoc function to establish a support vector machine (SVM) model, specifically designed for multi-class problems. We used the KernelFunction parameter of fitcecoc to select suitable kernel

functions (such as linear, polynomial, Gaussian, etc.) to accommodate different data structures and requirements. The SVM is a supervised learning algorithm grounded in statistical learning theory (Support vector machines, 2024). Its objective is to differentiate between data sets by identifying an optimal hyperplane. In typical classification challenges, it's crucial to delineate the boundary separating different data categories. Given the complexity of these boundaries and the multitude of potential solutions, SVM's core advantage lies in its ability to identify the most effective boundary. It accomplishes this by selecting a hyperplane that maximizes the margin between itself and the nearest data points from each category, thus enhancing the model's robustness to noise. SVMs are categorized into two types: "linear SVMs," for linearly separable data, and "non-linear SVMs," for data that cannot be separated by a straight line.

The mathematical model of the multiclass support vector machine (SVM) primarily consists of two major parts: the objective function and

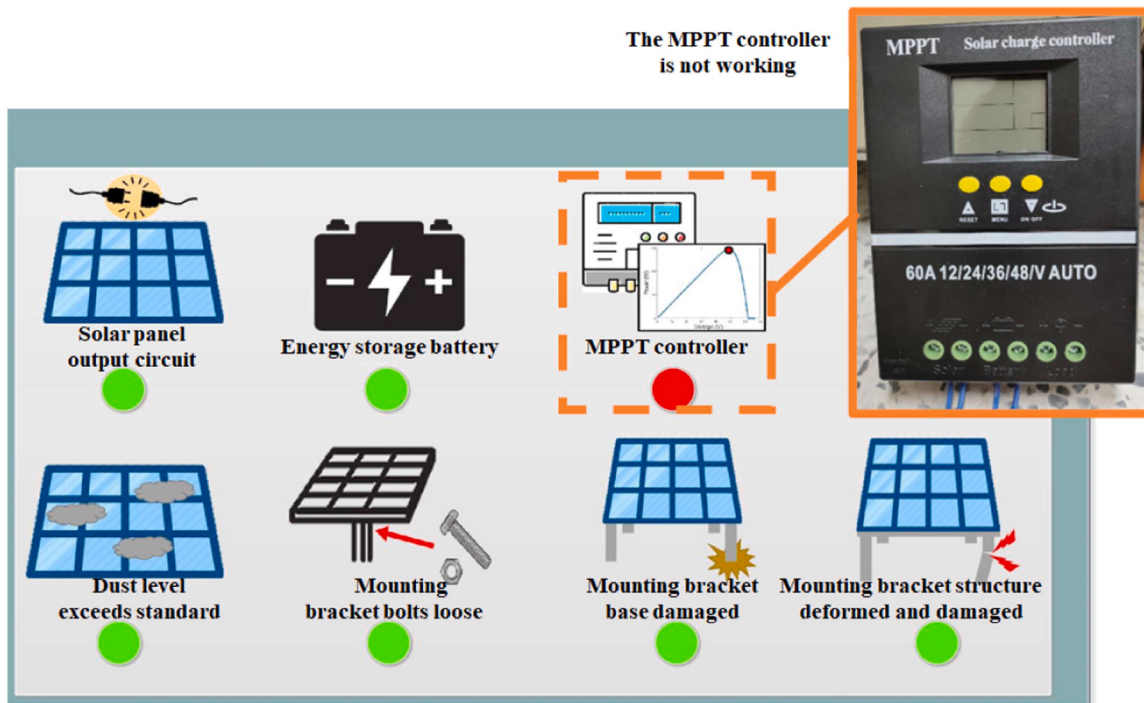


Fig. 23. The system platform's fault diagnosis indicates an MPPT controller fault.

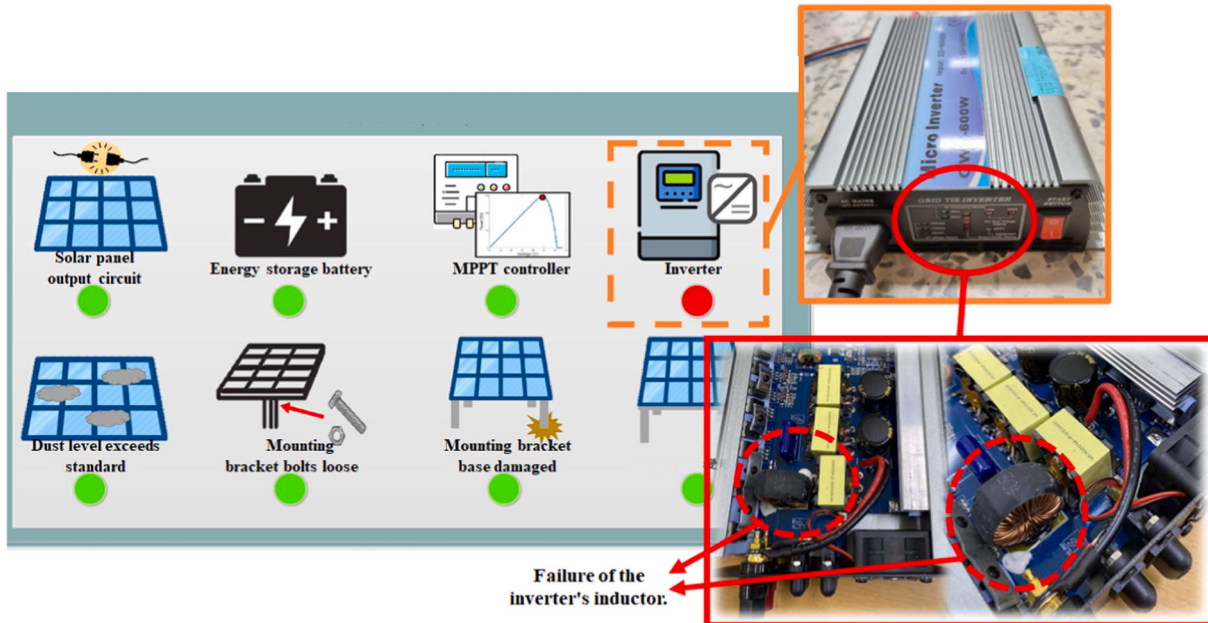


Fig. 24. The system platform's fault diagnosis indicates an inverter fault.

the constraints. The objective function aims to minimize the error rate of classification, while the constraints are designed to control the complexity of the SVM model, ensuring the model's generalization ability. Assuming there are k categories, n samples, and each sample has b -dimensional features, the objective function and constraints of this multiclass SVM can be collectively represented as Eq. (14).

$$\min_{w,b,\xi} \frac{1}{2} \sum_{k=1}^k \|w\|^2 + C \sum_{i=1}^n \sum_{k=1}^k \xi_i$$

$$\text{Subject to } y_i(w_k x_i + b_k) \geq 1 - \xi_{i,k}, \text{ for } \xi_{i,k} \geq 0, \quad 1 \leq i \leq n,$$

$$k = 1 \leq k$$

Herein, y_i represents the true label of the i th sample, ξ_i denotes the slack variable, C is the regularization parameter, w_k and b_k respectively represent the weight vector and bias of the hyperplane corresponding to the k th category, and $\xi_{i,k}$ indicates the slack variable of the i th sample under the k th category.

4.2.3.2. Solar PV array fault detection method. In the research on the fault detection method for solar PV arrays, this experiment employed array configurations of 2 (series) \times 4 (parallel) and 3 (series) \times 3

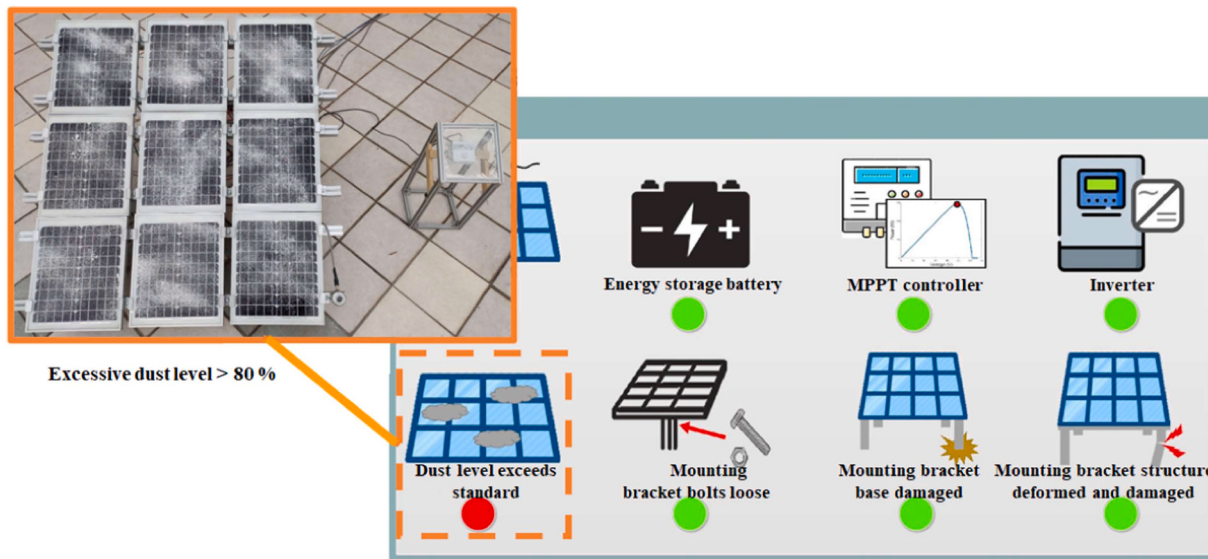


Fig. 25. The system platform's fault diagnosis indicates that the dust level is excessive.

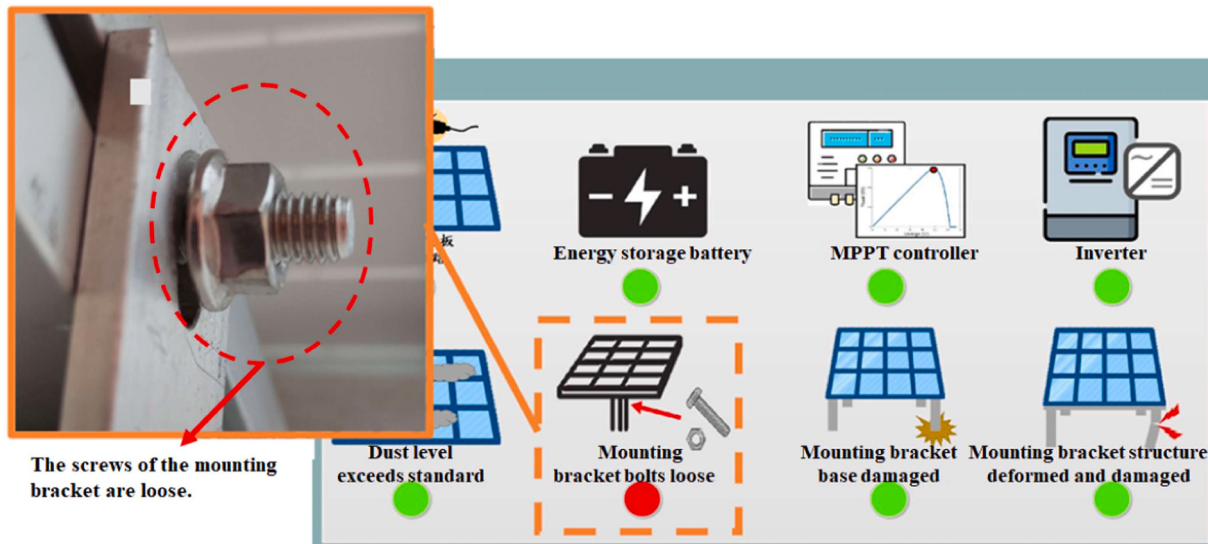


Fig. 26. The system platform's fault diagnosis indicates that the mounting bracket screw has loosened.

(parallel) for testing (Ma et al., 2018), as shown in Fig. 14 (a) and 14 (b). Additionally, voltmeters and ammeters were specially installed in the experiment to facilitate fault diagnosis. The primary detection targets included short circuits and open circuits in bypass diodes, as well as open circuit faults in the wiring, successfully determining the optimal installation positions for the voltmeter and ammeter.

Set against the context of Fig. 14(a), this document offers an in-depth analysis of readings obtained from voltmeters and ammeters. In situations where the solar panel array is functioning optimally without any malfunctions, the readings from the differential voltage sensors (specifically V₁ and V₂) will maintain a zero value. This phenomenon occurs because all modules within the solar PV panel array operate at the same maximum power voltage. In contrast, during malfunctions, there is a notable voltage disparity between the defective and operational modules. Should the solar PV panel array maintain normal operation, the ammeter will reflect current values that align with the prevailing solar conditions. In the case of a short circuit fault within the bypass diode, the current readings from the solar array will be consistent with those observed under normal conditions. Conversely, if a wire breakage (or

open circuit) transpires, the reading on the ammeter will drop to zero. Furthermore, should an open circuit fault in the bypass diode occur simultaneously with shading, the affected module will become a resistive load, harnessing energy produced by the other modules. In instances of significant shading, this leads to an energy disconnect, redirecting flow towards the defective module and consequently, the fault current reading for that module string will near zero, as depicted in Fig. 15.

Introduction to the operating principle: Under standard conditions, a solar PV array configured in 2 series × 4 parallel operates at the maximum power point (MPP) voltage (i.e., 36 V) with solar irradiance of approximately 300 W/m². At this point, the readings from the voltage sensors (V₁ and V₂) are both zero, as shown in the normal operating curve of the solar panel in Fig. 16. When a bypass diode short-circuit fault occurs in the PV panel (1), as illustrated in Fig. 17, the voltage at the MPP drops to 18 V. Under the same solar irradiance of 300 W/m², the measured short-circuit curve of the solar panel's bypass diode is presented in Fig. 18.

In PV panel (1), an open circuit fault in the bypass diode is illustrated in Fig. 19. Under such conditions of an open circuit in the bypass diode,

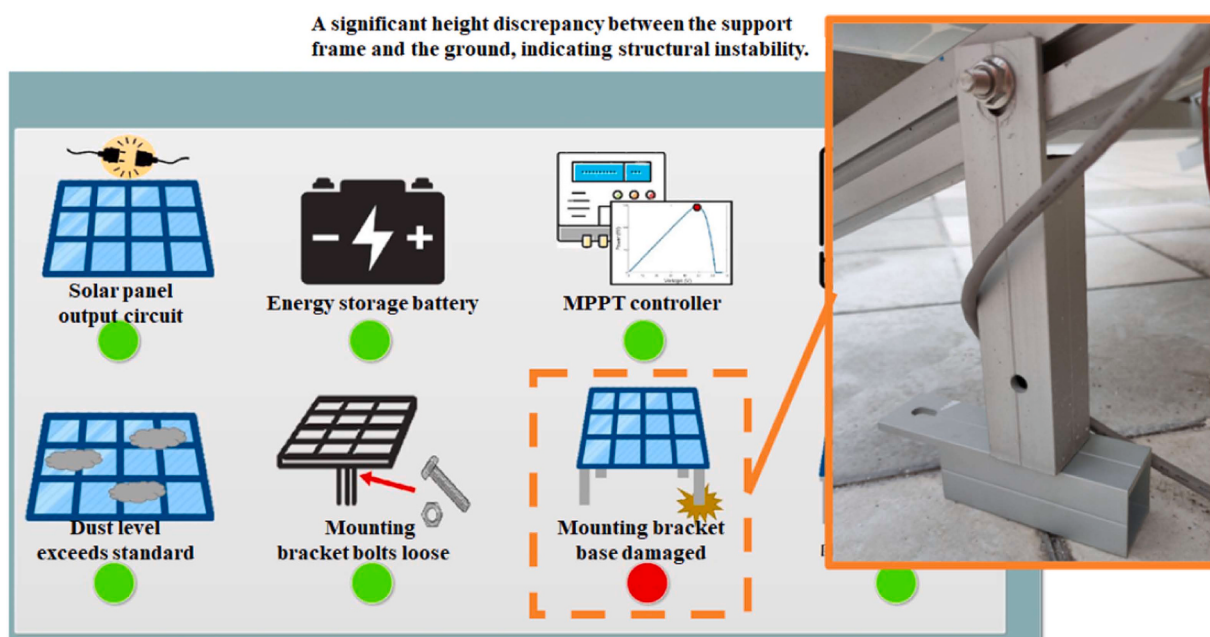


Fig. 27. The system platform's fault diagnosis indicates the mounting bracket's foundation has sustained damage.

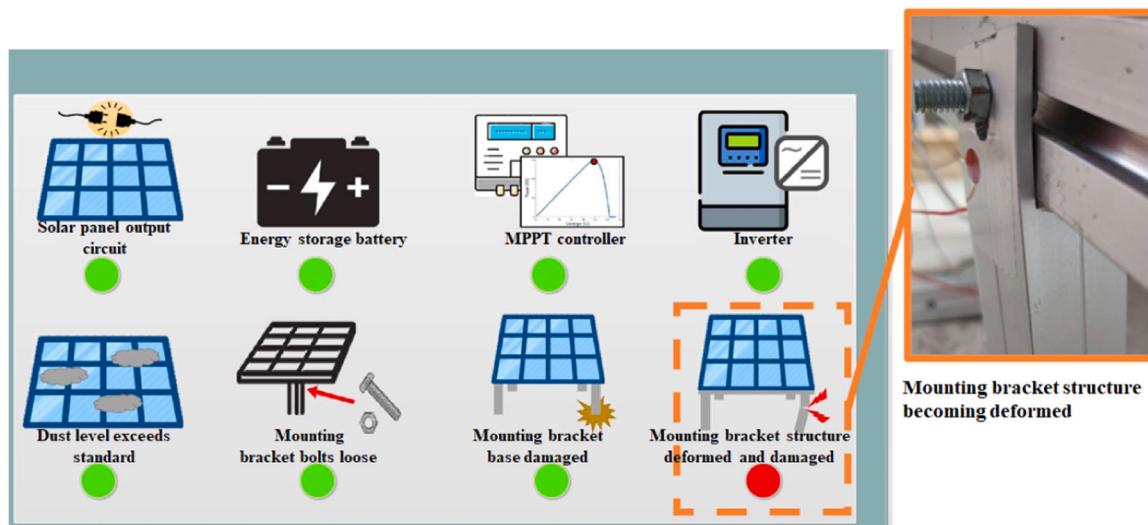


Fig. 28. The system platform's fault diagnosis indicates the mounting bracket structure has become deformed and damaged.

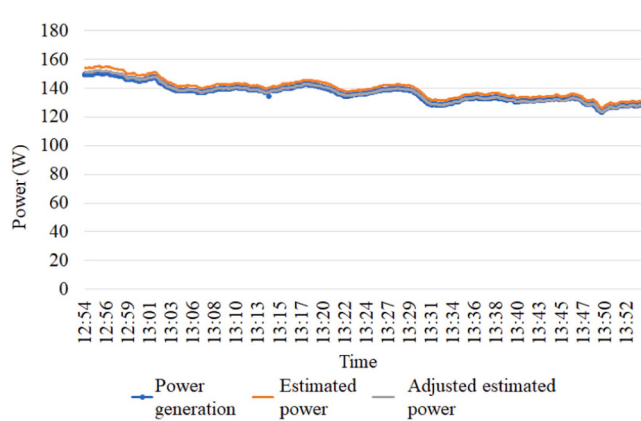


Fig. 29. Prediction of solar PV array power generation.

if subjected to solar irradiance of 300 W/m^2 , a temperature of 25°C , and shading conditions, the system's power generation efficiency will significantly decrease. Furthermore, the MPP voltage of a single PV panel will not be able to reach 18 volts (as shown in Fig. 18).

The ammeter is capable of measuring both open circuit faults and the open signal of bypass diodes. When an open circuit fault occurs, the current will not flow, leading to the inability of the module string to conduct electricity, as shown in Fig. 20. According to the definition of this study, if there is sunlight and the ammeter's reading remains at zero for a continuous period of 15 minutes, the situation is identified as an open circuit fault.

5. Experimental results

This section will validate the detection methods mentioned earlier and use PLC to collect data from various sensors. Subsequently, data processing, analysis, and presentation will be carried out through PLC,

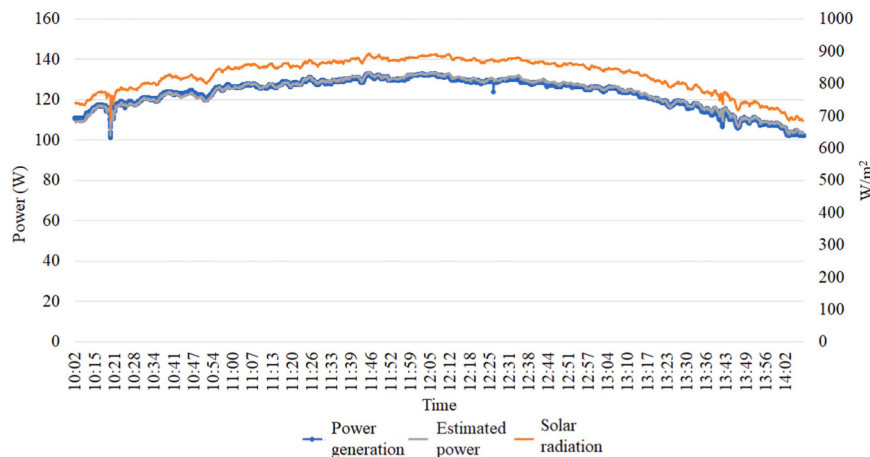


Fig. 30. Estimation of the actual power generation of the solar PV array within four hours.



Fig. 31. The actual images of solar PV arrays with flour quantities of 0 g, 20 g, and 50 g on the surface.

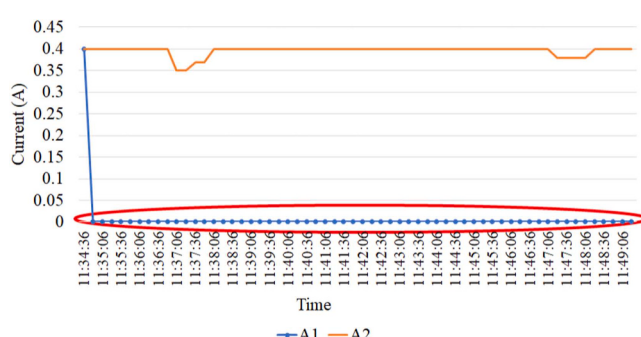


Fig. 32. Open circuit fault signal in solar PV array.

LabVIEW, and MATLAB.

5.1. Results of the PV system fault detection

The results of the PV system fault detection mainly cover eight types: solar PV panel output circuit faults, energy storage battery faults, MPPT controller faults, inverter faults, excessive dust accumulation, loosening of mounting frame screws, damage to the mounting frame foundation, and deformation or damage of the mounting frame structure.

Solar PV panel output circuit faults refer to anomalies in the connecting wires or connectors between the solar panels and the inverter, which can hinder the normal operation of the PV system or cause a decrease in power generation efficiency. The causes of such faults may include loosened or damaged connectors, broken wires, or poor contact, among others. The fault detection results presented by the system are

shown in Fig. 21, where a solar PV panel output circuit fault triggers a red warning light.

Possible causes of energy storage battery faults include loose connections in series or parallel battery circuits, over-discharge of the battery, insufficient charging, internal damage, or aging. These issues can prevent the battery from properly storing or releasing electrical energy, thereby impeding the normal operation of the solar power system. The fault detection results presented by the system are depicted in Fig. 22, where a red warning light is triggered by an energy storage battery fault.

The maximum power point tracking (MPPT) controller is designed to maximize the electrical output of solar PV panels. Potential causes of malfunction include damage to internal components, improper operation, or exposure to adverse environmental factors, such as excessively high or low temperatures, high humidity, or strong winds. Any of these conditions can lead to abnormal controller functioning. The fault detection results presented by the system are shown in Fig. 23, which displays a red warning light triggered by an MPPT controller fault.

The primary function of an inverter is to convert DC into AC. Numerous factors can lead to inverter failure, such as component damage, abnormal input or output voltages, overheating, or overload conditions. In the conducted tests, a notable discovery was damage to an inductor component, leading to an open circuit. The system presents fault detection results in Fig. 24, displaying a red warning light triggered by an inverter fault.

The criterion for excessive dust levels is set when the current power generation is reduced to below 80 % due to the impact of dust. Therefore, when the fault indicator light turns on, the solar PV panels should be cleaned immediately to ensure their surfaces remain clean and operate efficiently. The system presents fault detection results in Fig. 25, displaying a red warning light triggered by excessive dust levels.

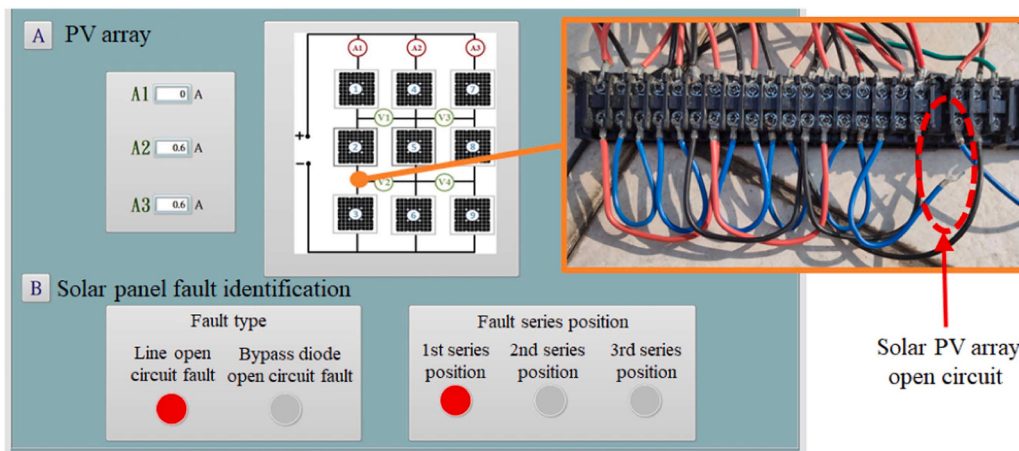


Fig. 33. Solar PV array open circuit fault warning.

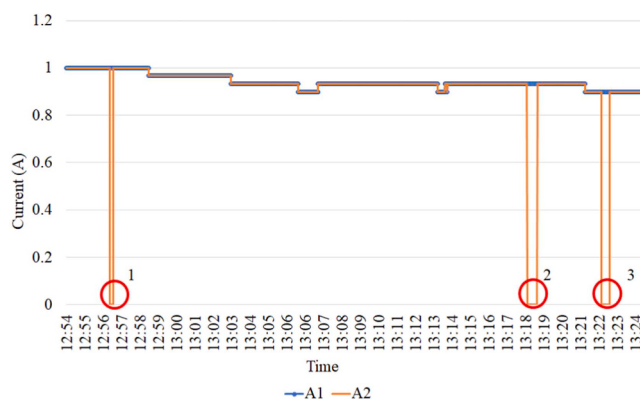


Fig. 34. Current signal of bypass diode open circuit fault.

Mounting bracket screws becoming loose typically refers to the screws, nuts, and other fastening components on the support frames of solar systems loosening due to long-term exposure to rainwater erosion or the impacts of typhoons and other severe weather conditions. This issue can further affect the operational efficiency and safety of the solar panels. The system presents fault detection results in Fig. 26, displaying a red warning light triggered because the mounting bracket screw has loosened.

Damage to the mounting bracket's foundation is commonly caused

by factors like subsidence, soil softening, and erosion beneath the support frames of solar systems. These conditions can lead to instability in the solar system's support structure, negatively impacting the operational efficiency and safety of the solar panels. Observations from experiments have shown a significant height discrepancy between the support frame and the ground, indicating structural instability. The system's fault detection results are presented in Fig. 27, which shows a red warning light triggered due to damage sustained by the mounting bracket's foundation.

Deformation and damage to the mounting bracket structure are primarily caused by the solar system's support frames enduring long-term exposure to wind loads, snow loads, and their own weight. These conditions can lead to structural deformation or damage, with the connection points of the support beams being the most susceptible to damage. In experiments, bending issues with the support beams were observed. The system's fault detection results are presented in Fig. 28, which shows a red warning light triggered due to the mounting bracket structure becoming deformed and damaged.

5.2. Solar PV panel dust accumulation detection results

To simulate the impact of dust in real-world conditions, this experiment used flour as a substitute for dust. The effect of dust on the efficiency of solar power generation was measured by comparing the changes in sunlight intensity recorded by a pyranometer and a light sensor placed under tempered glass. Through this measurement method,

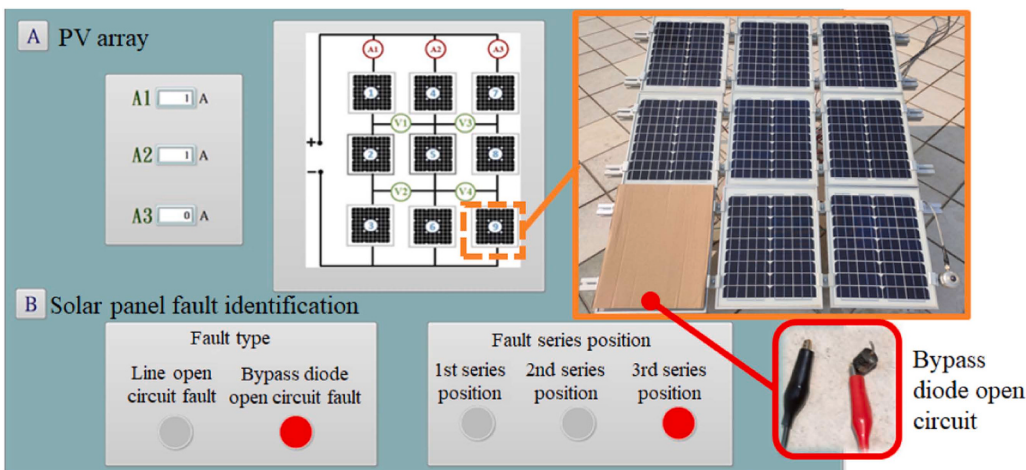


Fig. 35. PV panel (9) bypass diode open circuit fault warning.

Table 2Open circuit fault data of bypass diodes in a 3×3 solar PV array.

	Voltage meter (V1) measurement data	Voltage meter (V2) measurement data	Voltage meter (V3) measurement data	Voltage meter (V4) measurement data
Bypass diodes for PV panels (1)-(9) are all functioning normally	0.5 V	0.5 V	-0.1 V	-1.1 V
Open circuit fault in the bypass diode of PV panel (1)	14.1 V	9.1 V	-0.7 V	-2.4 V
Open circuit fault in the bypass diode of PV panel (2)	-5.3 V	9.1 V	-0.8 V	-2.7 V
Open circuit fault in the bypass diode of PV panel (3)	-5.2 V	-10.8 V	-0.9 V	-2.8 V
Open circuit fault in the bypass diode of PV panel (4)	-12.6 V	-6.8 V	13.5 V	6.5 V
Open circuit fault in the bypass diode of PV panel (5)	5.8 V	-6.7 V	-5.4 V	6.7 V
Open circuit fault in the bypass diode of PV panel (6)	5.6 V	11.5 V	-5.5 V	-12.4 V
Open circuit fault in the bypass diode of PV panel (7)	0.9 V	1.6 V	-14.2 V	-9 V
Open circuit fault in the bypass diode of PV panel (8)	0.9 V	1.7 V	4.5 V	-9 V
Open circuit fault in the bypass diode of PV panel (9)	0.8 V	1.6 V	4.5 V	9.3 V

5.3. Results of fault localization testing for solar PV arrays

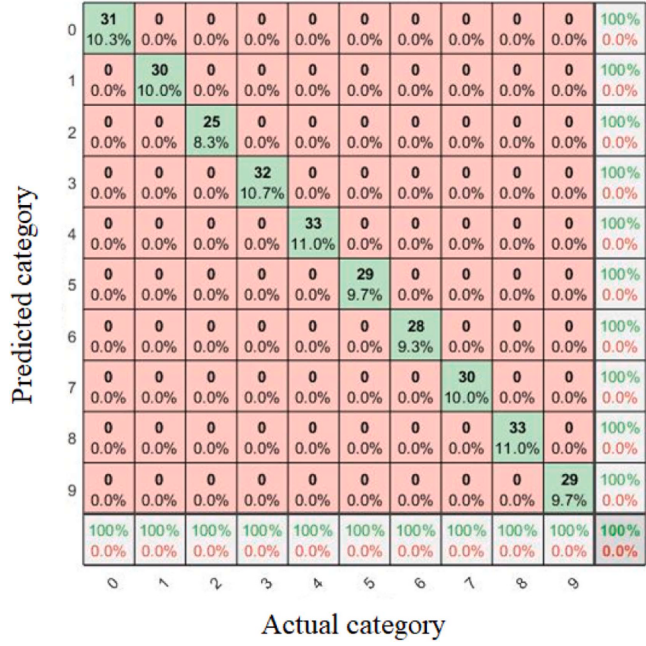


Fig. 36. Identification results for open circuit faults in bypass diodes of a 3×3 solar PV panel array.

we can estimate the degree to which dust accumulation reduces the efficiency of solar PV panels.

Through actual testing, we obtained the power generation curve of the solar PV array and further revised the K value in the prediction Eq. (13). The K value serves as a correction factor in the equation, taking into account factors such as the aging of solar PV panels over time, energy loss during transmission, and the efficiency of the MPPT controller, making it a necessary adjustment. The corrected curve is shown in Fig. 29, while the data from the corrected 4-hour test is displayed in Fig. 30.

This study will explore the effect of different amounts of flour on the power generation of nine solar PV arrays. we present experimental images of the solar PV arrays with surface flour amounts of 0 g, 20 g, and 50 g, as depicted in Fig. 31.

When the system operates, it automatically records data in both Excel and My Structured Query Language (MySQL) databases. If the ammeter displays zero for a continuous 15-minute period, as shown in Fig. 32, the system will backtrack from the 15th minute when the issue was detected to the initial 15 minutes when the fault occurred and record the data from this period. Simultaneously, the system's fault indicator light will illuminate, serving as a warning to the monitoring personnel that an open circuit fault has occurred, as detailed in Fig. 33.

Fig. 34 shows a situation in a solar PV array where a bypass diode experiences an open circuit fault, causing the current value to drop to zero. If such an anomaly occurs three times consecutively or more, the system will diagnose it as a bypass diode open circuit fault. In this case, it is the PV panel (9) that has experienced a bypass diode open circuit fault, as detailed in Fig. 35.

The open circuit fault in bypass diodes cannot be accurately determined through current measurements in the solar PV array, hence the need to use voltmeters installed within the array to locate the faults. In a 3×3 array, whether in normal PV panels or in panels (1) to (9), occurrences of open circuit faults in bypass diodes are recorded as voltage differences. Table 2 presents relevant data on open circuit faults in bypass diodes within a 3×3 solar PV array, listing the voltage values measured at different locations where the diode faults occurred.

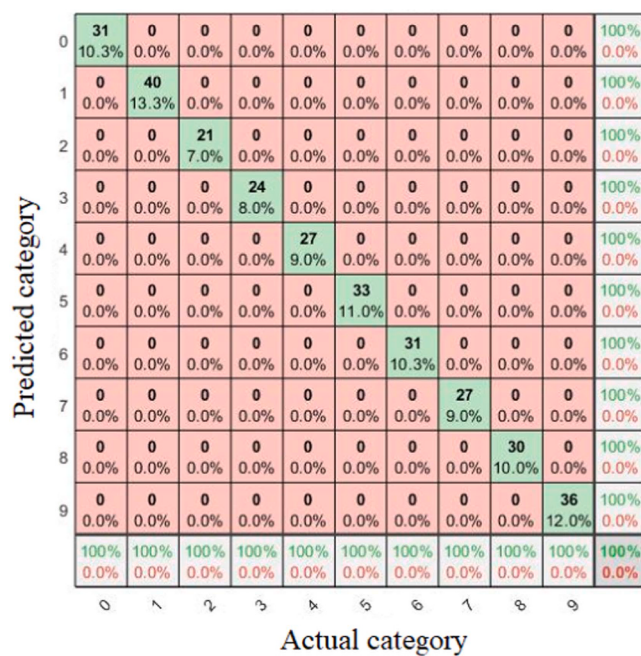
Table 2 shows the numerical differences for each solar panel when a fault occurs, revealing a certain regularity in the data. This regularity stems from variations in the hardware of the photovoltaic panels and their theoretical changes. By utilizing support vector machine (SVM) technology, we are able to pinpoint the exact location of faults, thereby achieving the goal of automated fault localization. In a 3×3 solar PV panel array, specifically for open circuit faults in bypass diodes, we collected a total of 1000 data points. Of these, 70 % (or 700 data points) were randomly selected for training, with the remaining 30 % (or 300 data points) used for testing. The identification results are presented in Fig. 36. In the confusion matrix, number 0 indicates a normal state, number 1 corresponds to PV panel (1), number 2 corresponds to PV panel (2), and so on, as shown in the solar panel positions in Fig. 14(b).

The detection of short-circuit and open-circuit faults in bypass diodes uses the same method, namely, identification through voltage differences measured by a voltmeter. However, there's a significant difference between short-circuit and open-circuit faults in bypass diodes: an open-circuit fault requires both the diode to be open and shading conditions, whereas a short-circuit fault can be detected anytime there is a diode

Table 3

Short-circuit fault data of bypass diodes in a 3×3 solar PV array.

	Voltage meter (V1) measurement data	Voltage meter (V2) measurement data	Voltage meter (V3) measurement data	Voltage meter (V4) measurement data
Bypass diodes for PV panels (1)–(9) are all functioning normally	0.5 V	0.5 V	-0.1 V	-1.1 V
Short circuit fault in the bypass diode of PV panel (1)	16.1 V	14.2 V	0 V	-4 V
Short circuit fault in the bypass diode of PV panel (2)	-1.4 V	14.2 V	0 V	-4.2 V
Short circuit fault in the bypass diode of PV panel (3)	-0.6 V	-1.6 V	0 V	-4.7 V
Short circuit fault in the bypass diode of PV panel (4)	-13.2 V	-5.6 V	16.6 V	6.2 V
Short circuit fault in the bypass diode of PV panel (5)	3.8 V	-6.6 V	-5.4 V	6.2 V
Short circuit fault in the bypass diode of PV panel (6)	6.9 V	12.5 V	-5.2 V	-15.8 V
Short circuit fault in the bypass diode of PV panel (7)	3.6 V	8.9 V	-16.4 V	-10.6 V
Short circuit fault in the bypass diode of PV panel (8)	4.3 V	8.8 V	5.4 V	-10.8 V
Short circuit fault in the bypass diode of PV panel (9)	4.1 V	8.5 V	5.3 V	11.2 V

**Fig. 37.** Identification results for short-circuit faults in bypass diodes of a 3×3 solar PV panel array.

short, making short-circuit faults in bypass diodes easier to detect and locate in practical applications. Data on short-circuit faults in bypass diodes within a 3×3 solar photovoltaic array are presented in **Table 3**.

Observations from the data in **Table 3** reveal a certain regularity in the variations, which stems from differences in the hardware of the solar PV panels and theoretical changes. By employing support vector machine (SVM) technology, we can accurately locate the fault. In the case of this 3×3 solar PV panel array, specifically for short-circuit faults in bypass diodes, we collected a total of 1000 data points. Of these, 70 % (or 700 data points) were randomly selected for training, while the remaining 30 % (or 300 data points) were used for testing. The identification results are displayed in **Fig. 37**.

Based on the identification results for both open and short circuit faults in bypass diodes, both achieved a 100 % accuracy rate. In this mixed case of short and open circuit faults in the bypass diodes of a 3×3

solar PV panel array, we collected a total of 1900 data points. Of these, 70 % (or 1330 data points) were randomly selected for training, and the remaining 30 % (or 570 data points) were used for testing. The overall fault identification results for the 3×3 solar PV panel array are shown in **Fig. 38**. In this overall fault identification, the confusion matrix's number 0 represents a normal state, numbers 1–9 correspond to the positions of short circuit faults in bypass diodes of PV panels (1) to (9), and numbers 10–18 correspond to the positions of open circuit faults in bypass diodes of PV panels (1) to (9).

Based on the identification results in **Fig. 38**, both the normal state and the short circuit and open circuit faults in bypass diodes can be clearly identified without being influenced by different types of faults. The recognition rate reaches 100 %, indicating that the data differences between faults are very significant, thus achieving highly accurate recognition results.

It is well known that different countries have varying electricity rates for peak and off-peak usage periods. In Taiwan, the location of this study, electricity usage is categorized into summer peak usage, summer off-peak usage, non-summer peak usage, and non-summer off-peak usage ([Taiwan power company electricity pricing information, 2024](#)). Specifically, the electricity price during the summer peak period is \$1.51 per kWh, and during the summer off-peak period, it is \$0.61 per kWh; the non-summer peak period price is \$1.49 per kWh, and the non-summer off-peak period price is \$0.59 per kWh. The difference in electricity rates between peak and off-peak periods is approximately 2.5 times. Additionally, solar power systems provide electricity during peak periods and utilize electricity supplied by the power company during off-peak periods, a model that helps reduce electricity costs. Furthermore, to enhance the stability and efficiency of solar power systems, this study developed a solar fault diagnosis strategy that employs sensors including a pyranometer, illuminance sensor, solar panel surface temperature sensor, ambient temperature sensor, inclinometer, accelerometer, strain gauge, as well as sensors for solar panel power generation, DC transmission, and AC grid supply data. The cost of these sensors is significantly lower than the expenses incurred from electricity usage, thereby offering considerable economic benefits from this research.

6. Conclusion

Firstly, this study focuses on exploring the common types of faults in PV modules and employs a fault diagnosis method for solar power systems based on machine learning technology, aiming to enhance the accuracy and efficiency of fault diagnosis. In this study, sensor signals

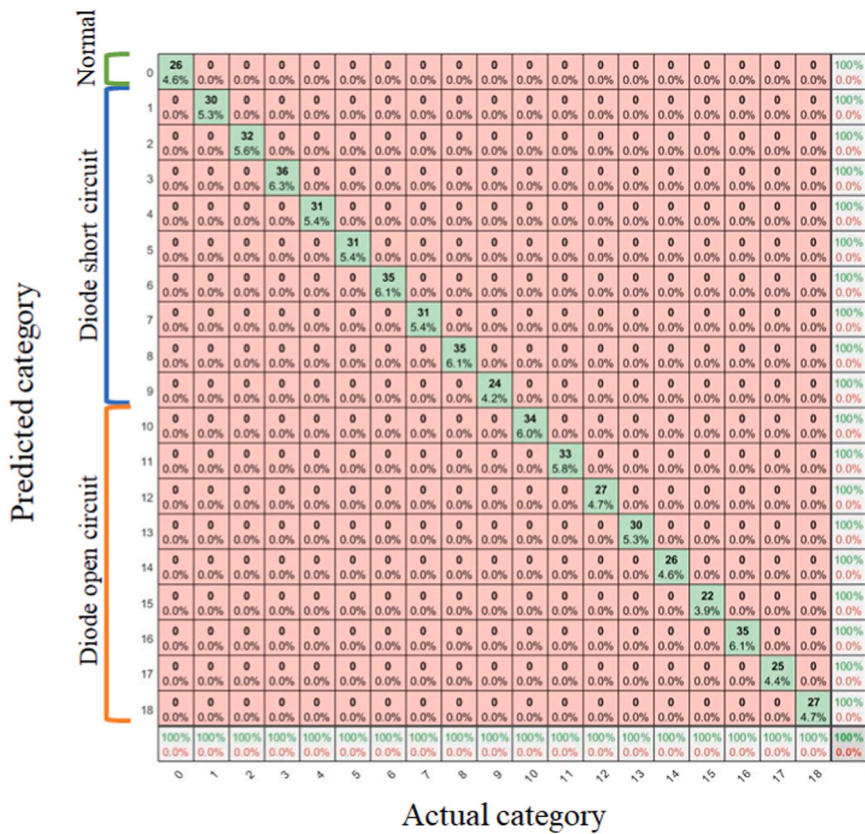


Fig. 38. Fault identification in a 3×3 solar PV panel array.

from the experimental platform were collected through a PLC, which initially processed the signals. Subsequently, the signals were further analyzed for fault diagnosis using graphical programming software such as LabVIEW and MATLAB. The sensor information and diagnostic results can be viewed through the onsite HMI, LabVIEW's data transmission network interface, and a web interface to monitor the system's operational status. Furthermore, the experimental results demonstrate that it is possible to successfully identify eight types of faults within the solar PV system: output circuitry of PV panels, energy storage batteries, MPPT controllers, inverters, dust accumulation, loosening of mounting rack screws, damage to the mounting rack foundation, and deformation of the mounting rack structure. Additionally, in the dust accumulation detection, employing MRA further narrowed the gap between the estimated power and the actual power output, indicating that the decrease in power output of the solar PV system under varying amounts of dust is significant. Lastly, by installing voltmeters and SVM within the solar PV array modules, it is possible to accurately measure and determine the type and location of short-circuit faults in bypass diodes. Similarly, by installing voltage and current meters within the array, it is possible to accurately measure and pinpoint the type and location of open-circuit faults in bypass diodes. The location of open-circuit faults in the circuit can be measured and determined by using an ammeter to identify their position in the series. In Taiwan, the electricity rates differ between peak and off-peak hours, with a difference of about 2.5 times. The fault diagnosis proposed in this study effectively enhances system stability. Moreover, this research has developed eight diagnostic functions, particularly suitable for environments in Taiwan with severe air pollution and frequent earthquakes, to ensure the stable operation of solar energy systems.

To further reduce research costs, this study utilized light sensors for experiments aimed at assessing the specific impact of dust accumulation on the power output of solar energy systems. However, the experimental results revealed significant differences between the data variation

curves recorded by light sensors and pyranometers, leading to biases in the system's prediction of power reduction due to dust. To enhance the accuracy of predictions and ensure the system's adaptability to operate under all-weather conditions, we recommend replacing the light intensity sensors with pyranometers. Through this improvement, not only can we achieve consistency in the data variation curves, but we can also fulfill the objective of measuring full daylight exposure, thereby significantly enhancing the system's efficiency and practical value.

CRediT authorship contribution statement

Chia-Chun Wu: Writing – original draft, Visualization, Validation, Software, Investigation. **Shiue-Der Lu:** Investigation, Formal analysis, Data curation, Conceptualization. **Hwa-Dong Liu:** Writing – original draft, Visualization, Validation, Supervision. **Meng-Hui Wang:** Writing – original draft, Visualization.

Declaration of Competing Interest

The authors declare that they have no known competing financial interests or personal relationships that could have appeared to influence the work reported in this paper.

Data Availability

No data was used for the research described in the article.

Acknowledgement

This work was supported by the National Science and Technology Council, Taiwan, under Grants NSTC 113-2221-E-167-046 and NSTC 113-2221-E-003-017.

References

- Alwar, S., Samitha, D., Boominathan, M.S., Balachandran, P.K., M.-Popa, L., 2022. Performance analysis of thermal image processing-based photovoltaic fault detection and PV array reconfiguration—a detailed experimentation (Nov.). *Energies* 15 (22), 8450. <https://doi.org/10.3390/en15228450>.
- Amer, H.N., Dahlani, N.Y., Azmi, A.M., Latip, M.F.A., Onn, M.S., Tumian, A., 2023. Solar power prediction based on artificial neural network guided by feature selection for large-scale solar photovoltaic plant (Nov.). *Energy Rep.* 5, 262–266. <https://doi.org/10.1016/j.egyr.2023.09.141> (Nov.).
- Anon, The relationship between dust accumulation on solar panels and power generation. (2024a), Available: (<https://reurl.cc/vkxODN>).
- Anon, The relationship between the azimuth angle and tilt angle of solar panels and their power generation. (2024b), Available: (<https://reurl.cc/KMzalj>).
- C.M., Nirmal Mukundan, Al-Durra, Ahmed, K., Vineeth, P., Jayaprakash, H. M. EL-Fouly, Tarek, Zeineldin, Hatem H., 2024. A new multilevel inverter with reduced component count for a standalone solar energy conversion system (Apr.). *IEEE Trans. Ind. Appl.* 60 (2), 3247–3262. <https://doi.org/10.1109/TIA.2023.3331672>.
- Cabral, D., Kosmadakis, G., Mathioulakis, E., 2024. Parametric comparison of a CPVT performance evaluation under standard testing procedures - ISO 9806:2017 and IEC 62108:2016 - for an automated and manual 2-axis tracking solar system stand (Jun.). *Energy Rep.* 9, 1242–1255. <https://doi.org/10.1016/j.egyr.2023.12.069> (Jun.).
- Dada, M., Popoola, Patricia, 2023. Recent advances in solar photovoltaic materials and systems for energy storage applications: a review (Jul.). *Beni-Suef Univ. J. Basic Appl. Sci.* 12 (66), 1–15. <https://doi.org/10.1186/s43088-023-00405-5> (Jul.).
- Duranay, Z.B., 2023. Fault detection in solar energy systems: a deep learning approach (Oct.). *Electronics* 12 (21), 4397. <https://doi.org/10.3390/electronics12214397> (Oct.).
- Govinda R. Timilsina, Lado Kurdegashvili, Patrick A. Narbel, A Review of Solar Energy Markets, Economics and Policies, Policy Research Working Paper, pp. 1–49, Oct. 2011. ([JMP Statistical Discovery LLC, Simple Linear Regression. \(2024\), Available: \(<https://reurl.cc/o0ba8V>\).

Khalil, E.A., Zeid, M.N.A., 2023. Computation of the environmental performance of ready-mix concrete for reducing CO₂ emissions: a case study in Egypt \(Nov.\). *Energy Rep.* 9, 144–148. <https://doi.org/10.1016/j.egyr.2023.09.125> \(Nov.\).

Least squares method \(2024\), Available: \(<https://reurl.cc/qkbEkg>\).

Liu, Q., Yang, B., Liu, Y., Ma, K., Guan, X., 2023. Collaborate global and local: an efficient PV compound fault diagnosis scheme with multilabel learning and model fusion \(Aug.\). *IEEE Trans. Instrum. Meas.* 72, 1–16. <https://doi.org/10.1109/TIM.2023.3300408>.

Ma, J., Bi, Z., Man, K.L., Dai, H., Wu, Z., 2018. Identification of partial shading in photovoltaic arrays using optimal sensor placement schemes. 2018 7th Int. Conf. Renew. Energy Res. Appl. \(ICRERA\), Paris, Fr. 458–462. <https://doi.org/10.1109/ICRERA.2018.8566715>.

Magableh, M.A.K., Radwan, A.A.A., Mohamed, Y.A.-R.I., 2024. Dynamic stabilization of a centralized weak grid-tied VSC system considering PV generator dynamics \(Jan.\). *IEEE Trans. Power Syst.* 39 \(1\), 2209–2226. <https://doi.org/10.1109/TPWRS.2023.3262811>.

Maka, Ali O.M., Alabid, Jamal M., 2022. Solar energy technology and its roles in sustainable development \(Jun.\). *Clean. Energy* 6 \(3\), 476–483. <https://doi.org/10.1093/ce/zkac023> \(Jun.\).

Multiple linear regression analysis. \(2024\), Available: \(<https://reurl.cc/AdWNLj>\).

Obaideen, K., Olabi, A.G., Swailmeen, Y.A., Shehata, N., Abdelkareem, M.A., Alami, A. H., Rodriguez, C., Sayed, E.T., 2023. Solar energy: applications, trends analysis, bibliometric analysis and research contribution to sustainable development goals \(SDGs\) \(Jan.\). *Sustainability* 15 \(2\), 6579. <https://doi.org/10.3390/su15021418> \(Jan.\).

Oni, A.M., Mohsin, A.S.M., Rahman, M.M., Bhuiyan, M.B.H., 2024. A comprehensive evaluation of solar cell technologies, associated loss mechanisms, and efficiency enhancement strategies for photovoltaic cells \(Jun.\). *Energy Rep.* 11, 3345–3366. <https://doi.org/10.1016/j.egyr.2024.03.007> \(Jun.\).

Salam, M.A., Shaikh, M.A.A., Ahmed, K., 2023. Green hydrogen based power generation prospect for sustainable development of Bangladesh using PEMFC and hydrogen gas turbine \(Dec.\). *Energy Rep.* 9, 3406–3416. <https://doi.org/10.1016/j.egyr.2023.02.024> \(Dec.\).

Selvaraj, T., Rengaraj, R., Venkatakrishnan, G., Soundararajan, S., Natarajan, K., Balachandran, P., David, P., Selvarajan, S., 2022. Environmental fault diagnosis of solar panels using solar thermal images in multiple convolutional neural networks \(Sep.\). *Int. Trans. Electr. Energy Syst.* 2022, 1–16. <https://doi.org/10.1155/2022/2872925> \(Sep.\).

Sun, X., et al., 2024. A cascaded multilevel modular energy router hybrid photovoltaic and energy storage with improved power balance capability \(Mar.\). *IEEE Trans. Power Electron.* 39 \(3\), 3637–3654. <https://doi.org/10.1109/TPEL.2023.3327684>.

Support vector machines \(2024\), Available: \(<https://reurl.cc/ykj7QO>\).

Taiwan power company electricity pricing information \(2024\), Available: \(<https://www.taipower.com.tw/upload/238/2024052013270121155.pdf>\).

Taiwan Yuasa battery, NP Type \(2024\), Available: \(<https://reurl.cc/eXoL0m>\).

Vijayan, D.S., Koda, E., Sivasuriyan, A., Winkler, J., Devarajan, P., 2023. Advancements in solar panel technology in civil engineering for revolutionizing renewable energy solutions—a review \(Sep.\). *Energies* 16 \(18\), 6579. <https://doi.org/10.3390/en16186579> \(Sep.\).

Voutsinas, S., Karolidis, D., Voyatzis, I., et al., 2023. Development of a machine-learning-based method for early fault detection in photovoltaic systems \(Apr.\). *J. Eng. Appl. Sci.* 70 \(27\). <https://doi.org/10.1186/s44147-023-00200-0> \(Apr.\).

Yuan, Z., Xiong, G., Fu, X., 2022. Artificial neural network for fault diagnosis of solar photovoltaic systems: a survey \(Nov.\). *Energies* 15 \(22\), 8693. <https://doi.org/10.3390/en15228693> \(Nov.\).

Zaidi, A., 2024. A bibliometric analysis of machine learning techniques in photovoltaic cells and solar energy \(2014–2022\) \(Jun.\). *Energy Rep.* 11, 2768–2779. <https://doi.org/10.1016/j.egyr.2024.02.036> \(Jun.\).](https://documents.worldbank.org/curated/en/546091468178728029/pdf/WPS5845.pdf#:~:text=URL%3A%20https%3A%2F%2Fdocuments.worldbank.org%2Fcurated%2Fen%2F546091468178728029%2Fpdf%2FWPS5845.pdf%0AVisible%3A%200%25%20)